Retinotopic organization of extrastriate cortex in a lemuriform primate, *Cheirogaleus medius*

Authors:
Martin I. Sereno[1,2,*], Monica Paolini[1,3], Richard Jeo[4,5], Allan Dobbins[4,6], John M. Allman[4]

Affiliations:
[1]Cognitive Science, University of California, San Diego, CA 92093
[2]Department of Psychology, San Diego State University, San Diego, CA 92182
[3]Senza Fili Consulting, 1425 Broadway #482, Seattle, WA 98122
[4]Division of Biology 216-76, California Institute of Technology, Pasadena, CA 92115
[5]Conservation International, 308 Tanglin Road, Singapore 247974, Singapore
[6]Department of Biomedical Engineering, University of Alabama, Birmingham, AL 35294

*Correspondence to: msereno@sdsu.edu

Keywords:
extrastriate cortex, retinotopy, evolution, parietal cortex, inferotemporal cortex

Abstract:
A unique opportunity allowed us to examine the retinotopic organization of visual areas in lateral extrastriate cortex of a primitive primate, the fat-tailed dwarf lemur (*Cheirogaleus medius*) using microelectrode receptive field mapping. The cortex was then physically flattened, cut parallel to cortical laminae, and stained to reveal myeloarchitecture. Retinotopic mapping data was analyzed with arrows diagrams and, after interpolation, visual field sign maps (Sereno et al., 1994). Despite the small overall size of the cortex in *Cheirogaleus*, it shows many similarities to other primates, including a well-defined MT, V2, DLa, VP, DM, FST, and a large retinotopically-organized posterior inferotemporal cortex. There are a number of differences. There does not appear to be an area with upper fields directly touching lower field V2 as in owl monkeys and marmosets. Posterior inferotemporal cortex contains a much more extensive representation of the periphery than is in found there in monkeys. Most intriguingly, there was an unambiguous duplication of the visual field near the center of gaze within architectonically-defined V1, V2, and MT that contained reversed visual field sign from that expected for each area (e.g., in mirror-image V1, the region is non-mirror-image, while in non-mirror-image MT, the region is mirror-image).

Main text:

A substantial portion of the neocortex in primates consists of visual areas, many of which are retinotopically organized (reviews: Sereno and Allman, 1991; Kaas and Krubitzer, 1991; Felleman and Van Essen, 1991). Old and New World monkeys share many features of the organization of extrastriate cortex. However, the organization of extrastriate cortex in many other primate groups, including most primitive primates as well as apes is much less well known.

To obtain a better picture of the evolution of cortical areas in primates and other mammals, it is crucial to distinguish features of the organization of extrastriate cortex common to all primates ('shared primitive features' for primates in the sense of the systematic biologist) from newly evolved features found only in certain subgroups of primates and not others ('shared derived features'). This information can only be determined by examining primates as well as other mammals from a range of different subgroups.

A comparative approach can often provide a broader perspective on functional studies initially performed in a single species. For example, when the cytochrome oxidase blobs were initially examined physiologically in squirrel monkeys and macaque monkeys, it appeared that they were specialized to process color (review: Hubel and Livingstone, 1988). The presence of cytochrome blobs in primitively nocturnal animals such as galagos and lorises (McGuinness et al., 1986; Preuss et al., 1996; Saraf et al., 2018) and cats (Anderson et al., 1988; Murphy et al., 1990), however, suggests that color processing may have arisen as an elaboration of cortical mechanisms initially specialized for processing object brightness that had already evolved in the nocturnal ancestors of day-living primates (Allman and Zucker, 1991; Preuss et al., 1996).

We were presented with a unique opportunity to experimentally examine the organization of extrastriate cortex in a primitive primate, the fat-tailed dwarf lemur, *Cheirogaleus medius*. Lemurs are a group of primates that retain many features thought to be primitive (Martin, 1990). Many are endangered and are found only on Madagascar. Their extrastriate areas have never been mapped in detail. Since the majority of visual areas are not graced with the convenient array of easily distinguishable anatomical features that characterize V1 and MT (e.g., prominent myeloarchitectonic borders), we turned to physiologically determined retinotopic organization as analyzed by visual field sign (Sereno et al., 1994) as the most comprehensive method of parsing the cortex into different areas in a single valuable subject.

The retinotopic organization of extrastriate visual cortex of the fat-tailed dwarf lemur revealed in this extensive mapping experiment showed many similarities to the retinotopic organization of extrastriate cortex in New World monkeys (Sereno et al., 1994; Sereno et al., 2015) as well as in Old World monkeys (Felleman and Van Essen, 1991), suggesting that much of the characteristic primate pattern of extrastriate organization dates to near the origin of primates. V1, V2, and MT in *Cheirogaleus*, for example, showed many similarities to V1, V2, and MT in other primates. The cortex surrounding MT also showed a number of similarities to areas in monkeys. There were several differences. One unusual feature was found near the center of gaze representations of V1, V2, and MT, entirely within the boundaries of those

architectonically-defined areas -- small duplicated regions containing reversed visual field sign from that expected for each of those areas. Also, posterior inferotemporal cortex was occupied by a large, myelinated area with much clearer retinotopic organization and ample peripheral representation compared to what is found in monkeys.

Materials and Methods

We recorded single- and multi-unit responses to visual stimuli from cortical areas in the right hemisphere of an anesthetized female fat-tailed dwarf lemur (*Cheirogaleus medius*) weighing 300 grams. This animal was obtained originally from the Duke Primate Center and was part of a captive breeding program undertaken in light of the destruction of its natural habitat in Madagascar. This animal had given birth to several offspring in captivity. Two months before the experiment, the animal presented with a fast growing tumor of the lower jaw. This tumor was deemed inoperable. It soon began to impede the animal's eating and it was determined by the attending veterinarian, Dr. Janet Baer, that the animal should be euthanized. The acute anesthetized recording experiment described below was undertaken after this decision had been made. The animal was euthanized at the end of the experiment.

Acute Mapping Experiment

The animal was deeply anesthetized and a craniotomy was made over lateral extrastriate cortex. A rod was cemented to the skull using several small stainless steel skull screws and Grip cement to allow the animal's head to be fixed during recording without soft-tissue pressure points. The dura was retracted and the cortex covered with a pool of warm viscous sterile silicone oil. The vascular pattern of the exposed cortex was photographed from a perpendicular viewpoint and the animal was tilted somewhat to keep the surface of the exposed cortex close to horizontal. The animal's body temperature was measured with a rectal probe and maintained with a warm water pad and a cloth cover. The animal was given 5% dextrose in saline subcutaneously to prevent dehydration. Care was taken to express urine accumulated in the bladder. Anesthesia was maintained for the duration of the experiment with additional doses of ketamine (1-3 mg/kg/hr i.m.) and butorphanol (0.4-1.2 mg/kg/hr i.m.; butorphanol is a synthetic opiate with 5 times the potency of morphine), or as needed to suppress muscular and heart rate response to stimuli. The depth of anesthesia of the unparalyzed animal was monitored continuously.

A stepping motor microdrive was positioned in the x-y plane of the exposed cortex with a manual micromanipulator while observing the brain surface and electrode tip through a dissecting microscope. Glass-coated platinum-iridium microelectrodes with 5-20 μm tip exposures were moved in the z-axis by a stepping motor microdrive designed by Gary Blasdel and Herb Adams (California Institute of Technology). Penetrations were typically made at points on a 250 μm grid in the x-y plane. For each penetration, the electrode tip was brought into contact with the pial surface of the cortex, and its location recorded on an enlarged photograph (20×) of the cortical vascular pattern. The electrode was then driven perpendicularly into the

cortex with the stepping motor microdrive to depths of approximately 700 μm. Small electrophysiological lesions were made at a number of sites (10 μA for 10 seconds at depths of 600 μm and 1300 μm at each site) during the experiment to allow us to relate the penetrations marked on the cortex photograph to architectonic features visible in the physically flattened, myelin-stained tissue.

Visual Stimulation

The animal monocularly viewed the interior of a translucent, plastic hemisphere 28.5 cm in diameter (one degree of visual angle equals 5 mm along the hemisphere surface) that was centered on the open left eye. The right eye was covered. The cornea was anesthetized with a long acting local anesthetic (0.7% dibucaine HCl dissolved in contact lens wetting solution). The pupil was dilated with Cyclogyl (1%). A thin ring supported by a fixable universal joint was cemented to the margin of the anesthetized cornea with a small drop (~10 μL) of Histoacryl cyanoacrylate tissue cement. The cornea was covered with a thin film of medium viscosity silicone oil to prevent drying. The local anesthetic wetting solution, pupil dilator, and silicone oil film were renewed at intervals during the experiment. This technique provides excellent stability of gaze because of the large size of the eye and the poor mechanical advantage of the posteriorly inserting eye muscles in this nocturnal animal. Paralysis is thus avoided making it easier to monitor and maintain the anesthetic state of the animal.

The blind spot and four other widely separated retinal blood vessel landmarks were plotted onto the plastic hemisphere by backprojecting their images with an on-axis ophthalmoscope. This procedure was aided by the highly reflective tapetum in this animal. These landmarks were checked repeatedly during the experiment to verify the fixation of gaze. The projected position of these landmarks were stable for the duration experiment (72 hours) to within the limits of accuracy of the back projection technique (≅1 deg). Because of the reflective tapetum, a quick check of the blood vessel position was also possible merely by briefly shining light from an optical fiber into the eye, which projects an image retinal blood vessels onto the hemisphere. The position of the receptive field for small clusters of neurons at each cortical recording site was plotted on the hemisphere. The border of each receptive field was carefully determined by testing many points around its circumference by projecting light and dark spots, bars, and texture patterns onto the outside surface of the hemisphere while listening to the amplified output of the electrode on an audio monitor. The person manipulating the electrode observed and verified the plotting of receptive field boundaries from the inside of the hemisphere. The hemisphere was dimly lit to avoid spurious responses due to diffuse light scatter. Overly bright stimuli were also avoided as these often tended to cause response suppression. Receptive fields were copied onto tracing paper made into a hemispherical shape by small, taped, radial folds after every 30-50 receptive fields had been plotted so that the plastic hemisphere could be cleared periodically (while leaving retinal landmarks) to avoid confusion.

Histology and Cortical Flatmount

At the end of the experiment, the animal with killed with an intraperitoneal overdose of Nembutal. The unfixed brain was immediately removed, quickly photographed, and then the cortex of both hemispheres was physically flattened (Tootell et al., 1985; Olavarria and van Sluyters, 1985; Sereno et al., 1994) by gently dissecting away the white matter with dry Q-tips. A cut in the fundus of the calcarine sulcus was made to allow the cortex to lie flat. The cortex was held in fixative (10% formalin) between large glass slides under a 30 gram weight for several hours. After that, the tissue was kept free floating in fixative. The tissue was infiltrated with 25% sucrose solution the day before sectioning. The flattened cortex of each hemisphere was sectioned in one piece parallel to cortical laminae at 50 μm on a freezing microtome (see Sereno et al., 1994, for additional details). Every section was stained using the Gallyas technique (1979) after drying sections in air for one day.

Regional variations in cortical thickness and flatness of the flatmount can result in one section passing through more than one cortical layer. Therefore, a composite drawing of the myelination pattern in 12 adjacent 50 μm sections was made with a microprojector (Aus Jena)

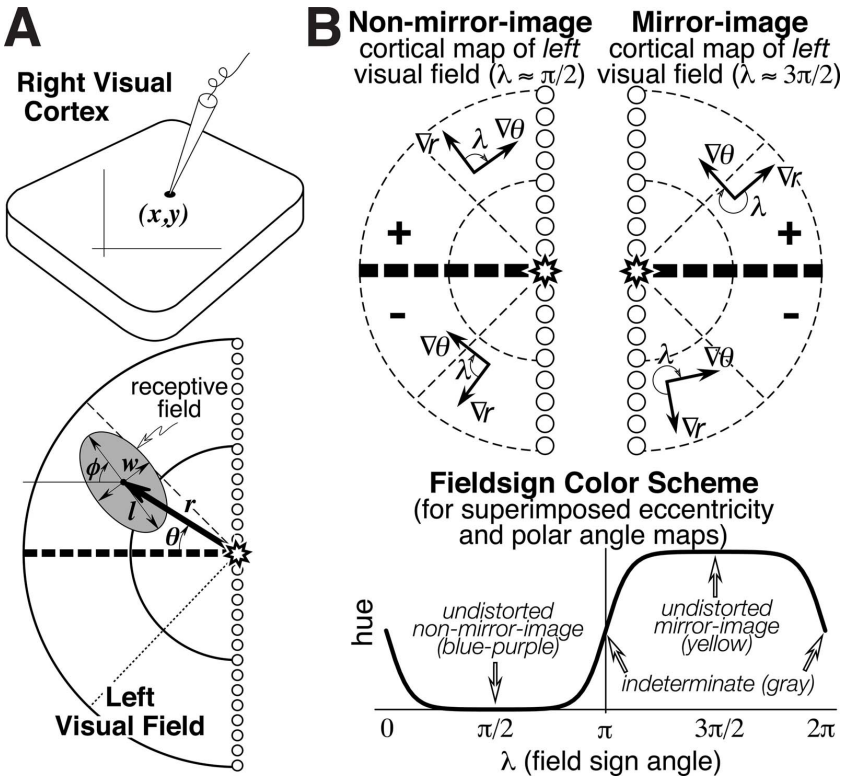

Figure 1. Seven parameters were digitized for each recording site. The location of the recording site was measured from the penetration photograph (x,y), the center of the receptive field is defined by its eccentricity and angle (r,θ), and the receptive field shape is parameterized by the length, width, and angle of the best-fitting ellipse (l,w,ϕ). An arrows diagram (see Fig. 5) is constructed by placing a small scaled copy of the arrow from the center of gaze to the receptive field center (thick arrow) at the position on the cortex from which that receptive field was recorded.

with a low power lens, and using radial cortical blood vessels and marker lesions to align each successive section with the drawing. This drawing was then scanned and annotated (see Fig. 9).

Digitization and Manipulation of Cortical Sites and Receptive Fields

A total of seven numbers were obtained for each named receptive field: the location of the recording site on the cortex (x,y), the eccentricity (r) and angle (θ) of the receptive field center relative to the center of gaze, and the length (l), width (w), and angle (ϕ) of the best-fitting receptive field ellipse (see Fig. 1). The receptive field coordinates were digitized by placing individual hemispherical paper data sheets back onto a spherical polar coordinate system drawn onto the plastic hemisphere. The center of gaze was placed at the 'North Pole' of the spherical polar coordinate system (Sereno et al., 1994).

Computer programs (available at http://www.cogsci.ucsd.edu/~sereno/.tmp/dist/rfutils/) converted the receptive field data files (ASCII tables) into six kinds of PostScript files: receptive field charts, numbered penetration charts, arrows diagrams, interpolated isoeccentricity and isopolar angle maps, and visual field sign maps. The isoeccentricity and isopolar angle maps were contoured and shaded using the GMT system (Wessel and Smith, 1991), a free software package (for Unix systems) for generating a number of different kinds of PostScript output maps from ASCII table inputs (available at https://www.soest.hawaii.edu/gmt/).

Flat hemifield charts represent radial distances (from the center of gaze) faithfully, but expand distances in a circumferential direction more and more as one moves away from the center of gaze; the circumferential stretching ranges from no distortion at the center of gaze up to a circumferential linear magnification of $\pi/2$ (~1.57×) at 90 degrees eccentricity. Each receptive field was therefore 'flat-corrected' on the planar visual field map by stretching it in a circumferential direction as a function of its eccentricity to accurately represent receptive field overlap and position of receptive field borders relative to isoeccentricity and isopolar angle landmarks on the flat hemifield chart.

The eccentricity and angle data were interpolated onto regular grids using a distance weighted smoothing technique (Lancaster and Salkauskas, 1986). The interpolated value ζ_j at the j^{th} *grid point* was the distance-weighted sum of the values, z_i, of all of the surrounding N data points, scaled by the sum of the weights:

$$\zeta_j = \frac{\sum_i^N z_i e^{-\alpha r_{ij}^2}/(r_{ij}^2 + \varepsilon)}{\sum_i^N e^{-\alpha r_{ij}^2}/(r_{ij}^2 + \varepsilon)}$$

where the weight for the i^{th} data point was an exponential function of the distance r_{ij} (in mm) between the i^{th} data point and the j^{th} grid point. The settings of ε and α adjust the stiffness of the interpolation. We used empirically derived settings for these parameters ($\varepsilon = 0.1$, $\alpha = 1.2$) shown in our previous work to be suitable for interpolating retinotopic data of this density (Sereno et al.,

1994). Before running the programs described above, a deformable template algorithm (Sereno et al., 1994) was first used to stretch the x-y locations of non-lesioned points taken from the photographed penetration map according to the final location of lesions in the stained, flatmounted tissue.

To superimpose the PostScript penetration map accurately on the brain drawing (see insets in Figures 4, 6-9, 13), we first overlaid a transparent high power (20×) photograph of the blood vessel pattern (with hand-marked penetrations) on the low power, electrode-view photograph of the brain taken just after the brain was removed, using the location of several large vessel junctions still visible on the unperfused brain.

For convenience, the angles of left hemifield receptive field centers are measured in a clockwise direction starting from the *left* horizontal meridian (the angle of the receptive field ellipse is treated similarly); thus a receptive field in the upper left visual quadrant will have an angle between 0 and 90 degrees, while a receptive field in the lower left visual quadrant will have an angle between 0 and -90 degrees (see Fig. 1).

Results

Myeloarchitecture

Figure 2 illustrates myelin-stained sections passing through the deeper layers of the cortex from the right (recorded) hemisphere as well as from the left (intact) hemisphere (left-right reversed or easier comparison). We have found that the myelination pattern revealed by a Gallyas stain is extremely robust throughout long recording experiments. The entire cortex including the hippocampus was flattened using relaxation cuts along the calcarine and the medial side of the frontal pole. Posterior is to the left and lateral is down in both Figures (see caption to Figure 8 for key to abbreviations).

V1 is clearly visible at the occipital pole (far left), as a distinct strip extending from the top to the bottom of both Figures. The regional variations reflect slight differences in the laminae through which the section plane passed.

V2 is visible, especially in sections through the lower layers of cortex, as a densely myelinated strip adjoining virtually the entire dorso-ventral extent of the anterior border of V1. V2 thins near the center of gaze. The anterior border of V2 is somewhat ambiguous superiorly. There are broad patchy variations in the density of the myelination in V2, most of which were difficult to attribute to variations in the flatness of the tissue since they extended through many sections.

MT appears as a prominent, densely myelinated oval on a line between the center of gaze of V2 and primary auditory cortex. It has a thin, somewhat less densely myelinated halo in this section. Laterally and anteriorly is a small triangular patch of cortex visually similar to FST in monkeys. Between MT and V2, there is a small myelinated patch, and further lateral to MT, in posterior inferotemporal cortex, there is an additional large patch of moderately dense myelination adjacent to FST.

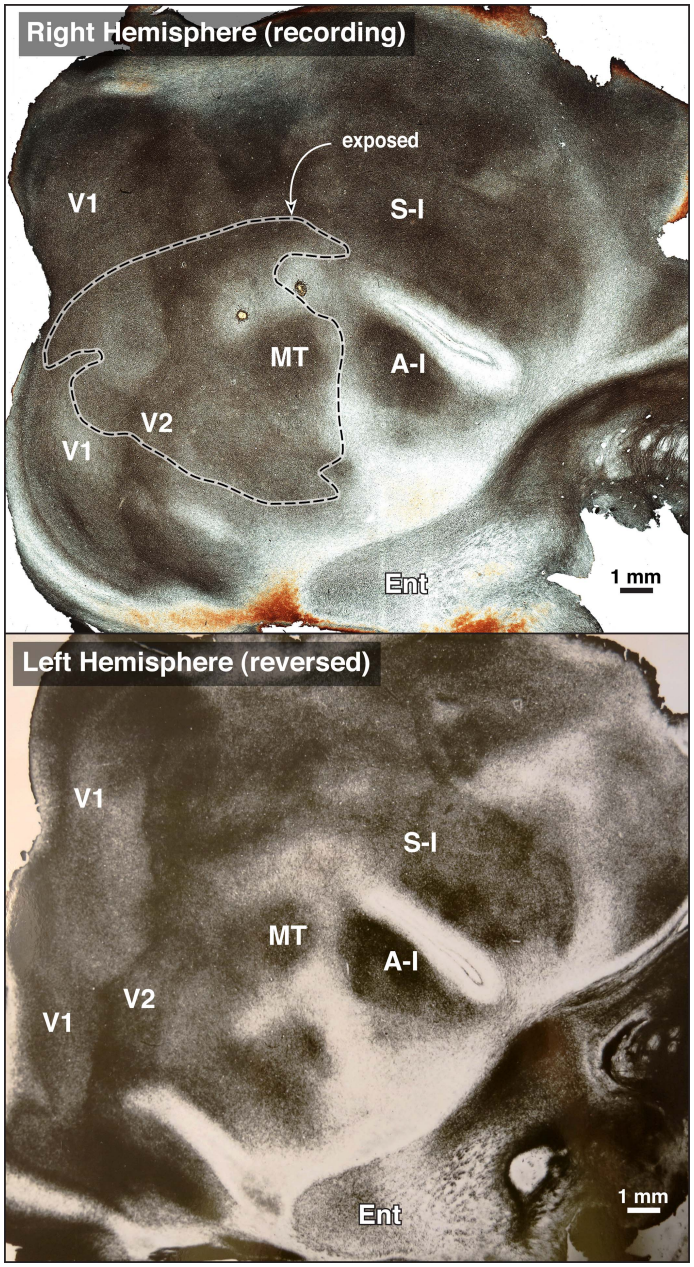

Figure 2. Physically-flattened myelin-stained cortex (Gallyas technique) from both hemispheres at level of infragranular layers. Dashed contour (top) shows electrophysiological recording region; non-recorded hemisphere (bottom) left-right reversed to ease comparison. The calcarine sulcus and frontal pole were incised to allow the cortex to lay flat (occipital pole left, lateral edge of cortex down). A hint of mottling in V1 may reflect less-myelinated blobs. V2 shows denser deep-layer myelination. MT is a densely myelinated circle with a thin halo posterior to more densely myelinated primary auditory cortex (A-I). Medial to MT (up) is a lightly myelinated region marked by two small lesions (blood clots). A similar lightly myelinated region is present in the other (unexposed) hemisphere. Medial to the lightly myelinated area are two anterior-posteriorly elongated heavily myelinated strips; the posterior part of the more lateral strip corresponds to DM. Lateral to MT is a large myelinated patch in posterior inferotemporal cortex (FST and ITc). The small Sylvian sulcus (between S-I and A-I) is very lightly myelinated because the section passes into more superficial cortical layers. Primary somatosensory cortex lies anterior and medial to the Sylvian sulcus. The anterolateral neocortex (down, right) is lightly myelinated even while more laterally-placed entorhinal cortex (Ent) is moderately myelinated.

Just medial to MT (up) is a region of very light myelination. In the center of this region in

the recorded hemisphere, there are two blood spots visible as small holes in the section. However, an unmyelinated region is present in an identical place in the opposite, unrecorded hemisphere, which argues against this unmyelinated region being an artifact of the electrophysiological recording. Medial to the lightly myelinated region, directly adjoining dorsal V2 are two parallel, rostrocaudally elongated bands of myelination. These bands extend almost to somatosensory cortex.

Anterior to visual cortical areas, primary auditory cortical areas are very densely myelinated and are separated from the visual areas by a very lightly myelinated region (this lightly myelinated region is buried in the superior temporal sulcus in New and Old World monkeys, which is absent in *Cheirogaleus*). Just anterior to primary auditory cortical areas is the nearly vertical Sylvian sulcus, which is very lightly stained, as a result of the section passing through more superficial cortical layers of the very thin cortex there. Anterior and medial to the Sylvian sulcus, several subregions of S-I are visible. The lateral margin of the neocortex is very lightly myelinated. Yet more lateral is moderately myelinated entorhinal cortex.

Recording Sites and Receptive Field Chart

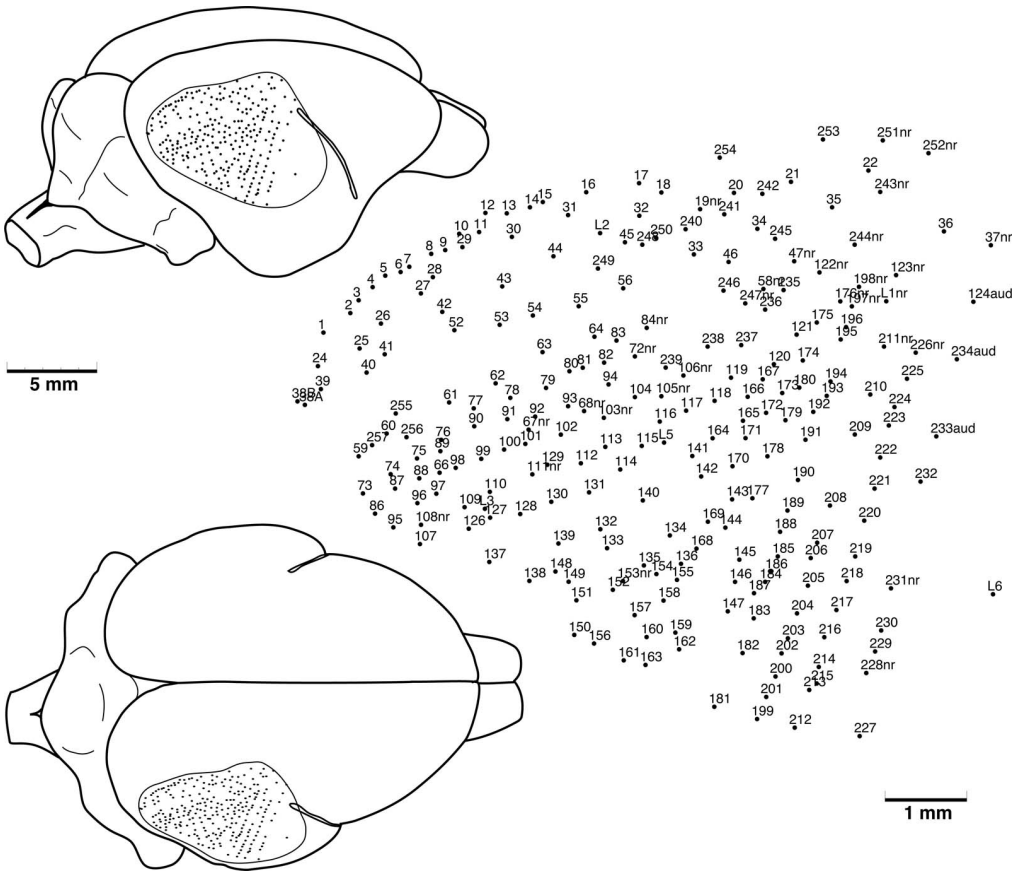

Figure 3. Location of 257 numbered recording sites in lateral extrastriate cortex of the right hemisphere of a fat-tailed dwarf lemur, *Cheirogaleus medius*. The correspondingly numbered receptive fields are shown in Figure 4A. Lower left inset shows recording sites in a dorsal view while upper left inset shows the sites in electrode view.

Figure 3 shows the location of 257 numbered recording sites in the right hemisphere of the cortex of the fat-tailed dwarf lemur, *Cheirogaleus medius*, on a recording-electrode view (top left) and a dorsal view (bottom left, right). The recording sites extended from dorsolateral to ventrolateral occipito-temporal cortex, and from V1 to the anterior border of visually-responsive cortex near the dorsal end of the small Sylvian fissure.

The corresponding receptive fields for the 217 visually responsive sites (out of 257 total recording sites) are shown in Figure 4. In figure 4A the receptive fields are drawn as transparent, labeled ellipses, while in Figure 4B, they are drawn in order of receptive field length and randomly assigned opaque shades to bring out some of the smaller receptive fields lost in the clutter near the center of gaze in Figure 4A. Penetration maps and corresponding numbered receptive field charts are only useful for illustrating very small subsets of retinotopic mapping data. We therefore applied two techniques better adapted to analyzing large retinotopic mapping

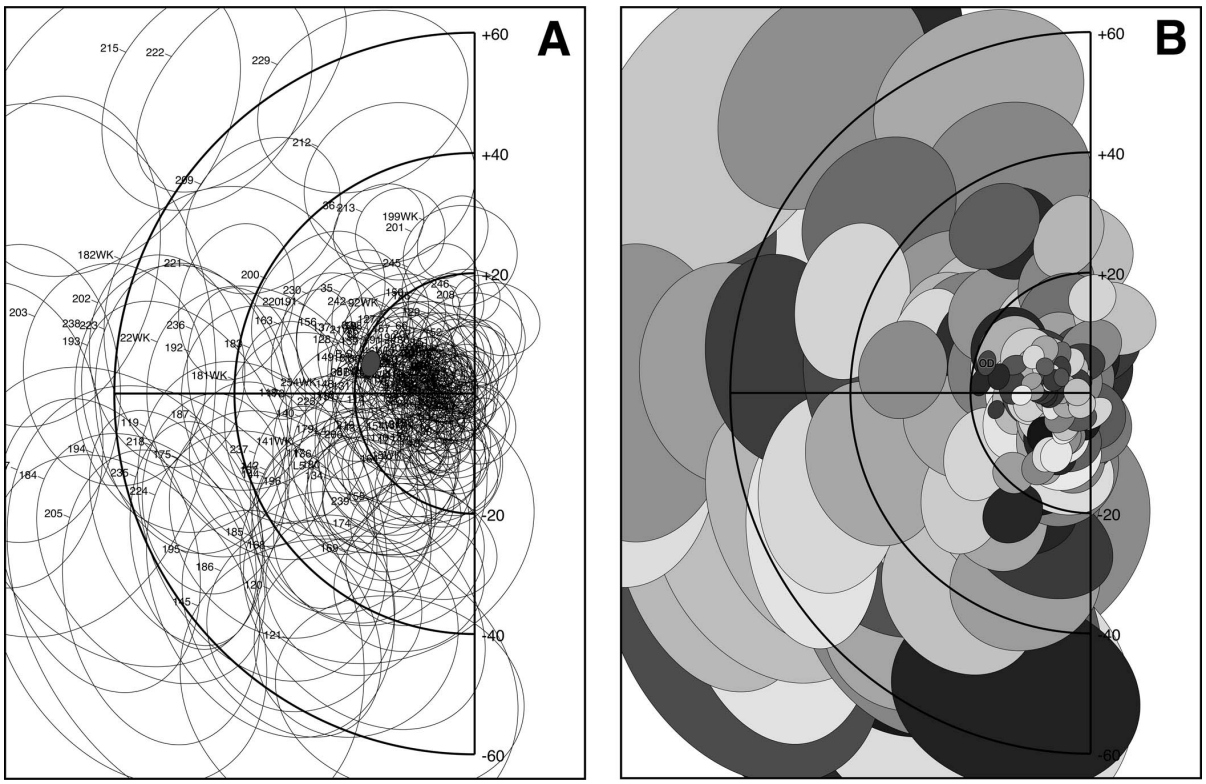

Figure 4. Location of 257 numbered recording sites in lateral extrastriate cortex of the right hemisphere of a fat-tailed dwarf lemur, *Cheirogaleus medius*. The correspondingly numbered receptive fields are shown in Figure 5A. The inset at the lower left shows the location of the recording sites on the brain in a dorsal view while the upper left inset shows the sites in an electrode view.

data sets -- *arrows diagrams* and *visual field sign maps* (Sereno et al., 1994; 1995) -- to the data set from Figures 3 and 4.

Arrows Diagram

One way to get an overview of large amounts of retinotopic mapping data is to indicate the visual field location of each *receptive field center* by placing a scaled arrow at each recording site. The angle and length of each arrow represents the angle and distance of the receptive field center with respect to the center of gaze (*not* direction selectivity). For example, a peripheral upper vertical meridian receptive field would be a long upward-pointing arrow while a horizontal meridian receptive field near the center of gaze would be a short leftward-pointing arrow.

The arrows diagram in Figure 5 illustrates all of the data from Figures 3 and 4. It is now possible to make out systematic changes in receptive field location as electrode penetration

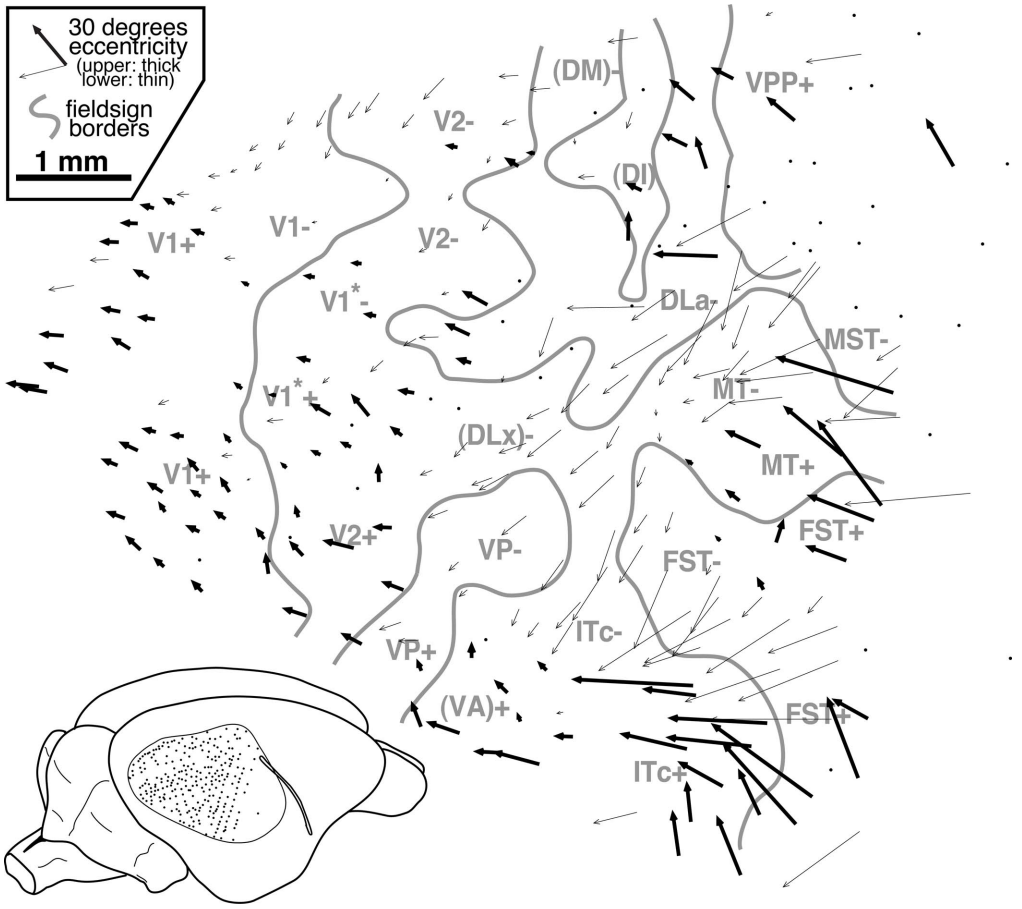

Figure 5. Arrows diagram of retinotopy data from Figures 3 and 4 illustrating visual field position of receptive field centers (arrow length and angle, thick arrows for upper field) and relative position of corresponding cortical recording sites (center of each arrow). Non-responsive penetrations are marked with a dot. Inset shows location of penetrations on the brain. Contours represent calculated visual field sign boundaries. For abbreviations, see Figure 8 caption.

sequences pass through multiple visual areas in dorsolateral extrastriate cortex (thick arrows for upper visual field, thin for lower; dots for non-visually responsive locations).

Several areas are apparent in this diagram. MT, for example, is visible at the far anterior edge of the exposure halfway between the medial and lateral edge as a patch of upper visual field

(thick arrows) lateral to a patch of lower visual field, with eccentricity (arrow length) increasing as one moves anteriorly and somewhat medially. Several additional retinotopically organized areas (smoothly changing arrow direction and length) are visible lateral to MT, and the general distinction between lateral upper fields and medial lower fields is obvious in the smaller arrows at the expanded representation of the center of gaze in V1 and V2.

Isoeccentricity and Isopolar Angle Contour Maps

Arrows diagrams faithfully represent the discrete nature of microelectrode retinotopic mapping data and make it possible to search for reversals in the entire data set without having to refer back and forth between a penetration map and a (large) set of receptive field charts. However, we have found that a *visual field sign map* (local mirror-image versus non-mirror image representation of the visual field -- see below) provides an even more intuitive way to divide the cortex up into areas on the basis of retinotopic mapping data. In order to calculate a visual field sign map, we first interpolate the sparse mapping data onto a regular x-y grid of cortical coordinates so that we can estimate the direction of the local cortical gradients in eccentricity and polar angle (see Materials and Methods).

Figure 6 shows a interpolated, shaded contour map of eccentricity, r, for the data shown in Figure 5. In this plot, the center of gaze (small eccentricities) is red, mid-eccentricities are blue, and the periphery is green. There is a general tendency in lateral extrastriate cortex for eccentricity to increase as one moves anteriorly. There is a pocket of small eccentricities (red) rostrally, which includes the center of gaze representation of MT near the far right. There are several peaks of large eccentricities (green) anteriorly, above and below MT. Interestingly, an eccentricity minimum appears to be situated entirely within architectonically defined V1 (see below).

Figure 7 shows an interpolated shaded contour map of receptive field polar angle, θ, for the same data. The lower field vertical meridian (-90 degrees) is green, the horizontal meridian (0 degrees) is blue, and the upper field vertical meridian (+90 degrees) is red. The upper field contour lines are dashed while the lower field contour lines are dotted. The map of polar angle is more complex than the map of eccentricity; there are a number of representations of the horizontal meridian (marked by thick dashed lines) as well as the upper and lower field vertical meridians. The anterior border of V1 is marked by a lower field vertical meridian (green) at the top middle and an upper field vertical meridian (red) near the bottom left of the figure. There is a second, arc-shaped lower field vertical meridian (green) at the middle right, part of which constitutes the posterior border of MT. There are several smaller upper field vertical meridian representations (red) at the lower, middle and upper right. The one in the middle forms the anterior border of MT.

By superimposing the r and θ contour plots from Figures 6 and 7, we can obtain a map of cortical retinotopy. This is essentially a smoothly interpolated representation of the arrow (vector field) map in Figure 5. Unfortunately, such a double contour map is difficult to read; there is no

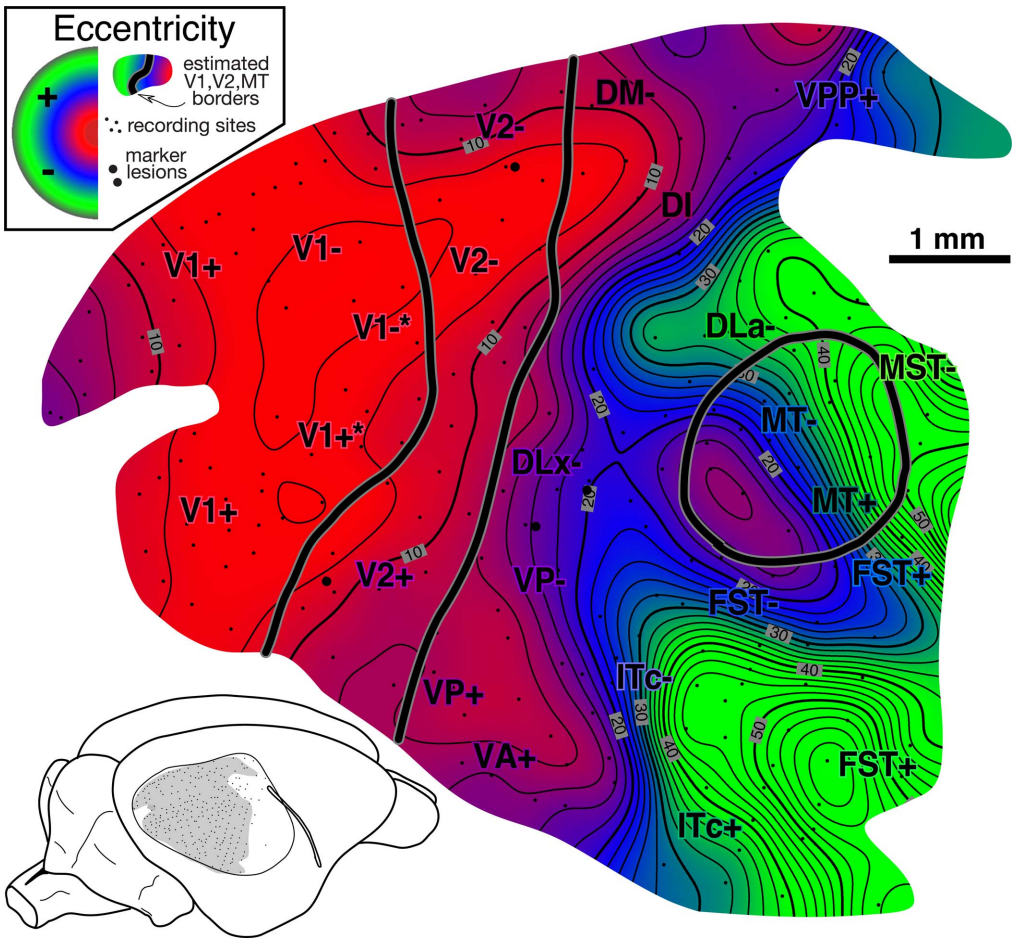

Figure 6. Cortical map of receptive field eccentricity for data from Figure 5. Central to peripheral visual fields are shaded red to blue to green. There is an eccentricity minimum (bright red) within the borders of V1 at the upper left of the Figure (see text). Eccentricity generally increases moving anteriorly (to right). There is a second eccentricity minimum just inside MT at the middle right. There are eccentricity maxima at the anterior border of MT and at the boundary between FST and ITc. To ease comparison, areal labels are placed in corresponding positions in Figures 6-8. The inset shows recording locations on the brain. For abbreviations, see Figure 8 caption.

way to color both contour maps at the same time, making it difficult to tell in which direction each set of contours is increasing. Distinct re-representations of the visual field and transitions between areas are not obvious. Finally, the positioning of the contours in these maps are sensitive to the positioning of the axes of the receptive field coordinate system -- which is always somewhat arbitrary because of the lack of retinal landmarks for the horizontal and vertical meridians (see discussion in Sereno et al., 2015). Visual field sign maps overcome all those difficulties.

Visual Field Sign Map

A local feature of each small patch of visual cortex is whether it contains a non-mirror-image representation of the visual field (e.g., V2) or a mirror-image representation of the visual

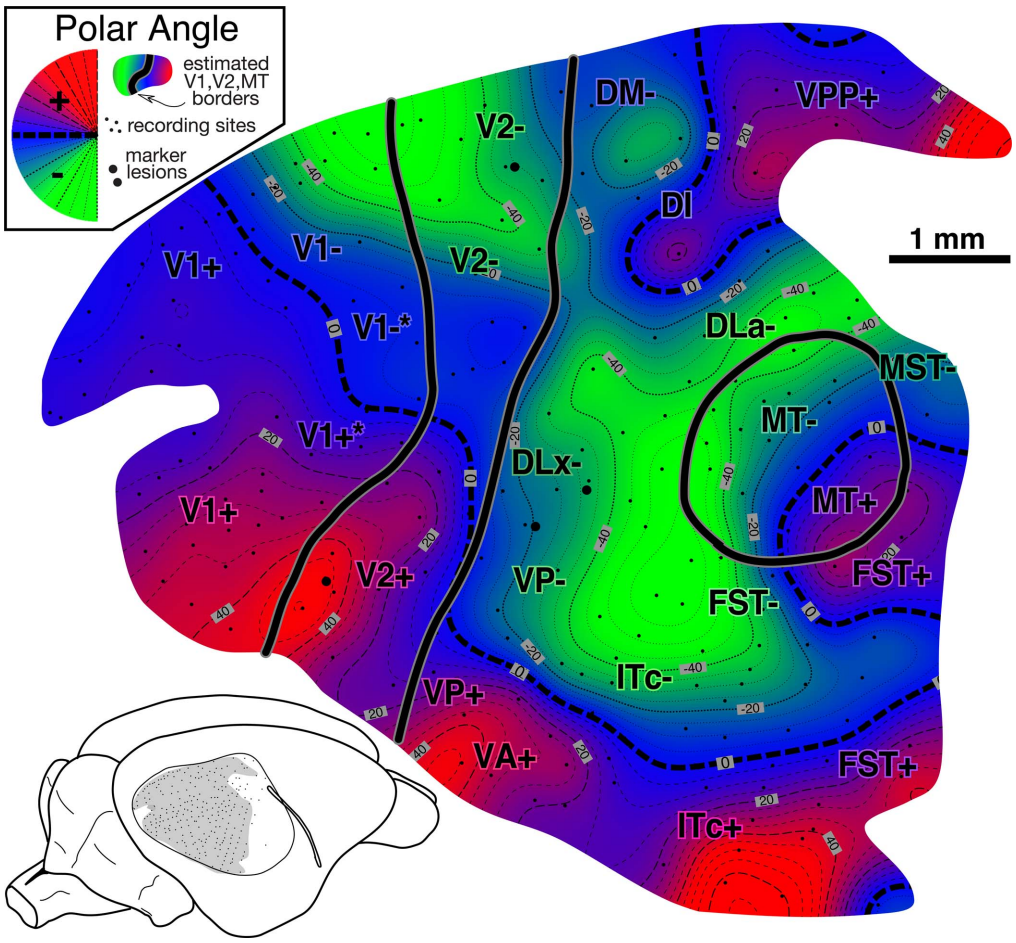

Figure 7. Cortical map of receptive field polar angle for data from Figure 5. The lower field vertical meridian is shaded green, the horizontal meridian is blue, and the upper field vertical meridian is red. The horizontal meridian is shown in bold dashed lines, upper field isopolar angle lines are shown as thin dashed lines, and lower field contour lines are even thinner dotted lines. The polar angle map is more complex than the eccentricity map. There are three upper vertical meridian representations along the bottom of the map (red), two lower vertical meridian representations (green) along the top of the map, a three-pointed lower vertical meridian (green) representation at the center, and two more upper vertical meridian representations (red) at the right edge. Most of these correspond to borders between areas in the visual field sign map. The inset shows recording locations on the brain. For abbreviations, see Figure 8 caption.

field (e.g., V1) when viewed from the cortical surface. This *local visual field sign* (non-mirror-image versus mirror-image) can be calculated for each cortical point given smoothed x-y maps of eccentricity and angle. More precisely, for each point on the cortex, we estimate the clockwise angle between the gradient in eccentricity, ∇r, and the gradient in polar angle, $\nabla \theta$, both with respect to cortical position. An angle between the gradients of $\pi/2$ signifies a locally undistorted (angle-preserving or conformal) non-mirror-image representation while an angle of $3\pi/2$ signifies an undistorted (conformal) mirror-image representation (Sereno et al., 1994). Intermediate angles signify different degrees of local non-orthogonality (non-conformality or shearing) of the visual field representation. There are singularities at 0 and π, where visual field

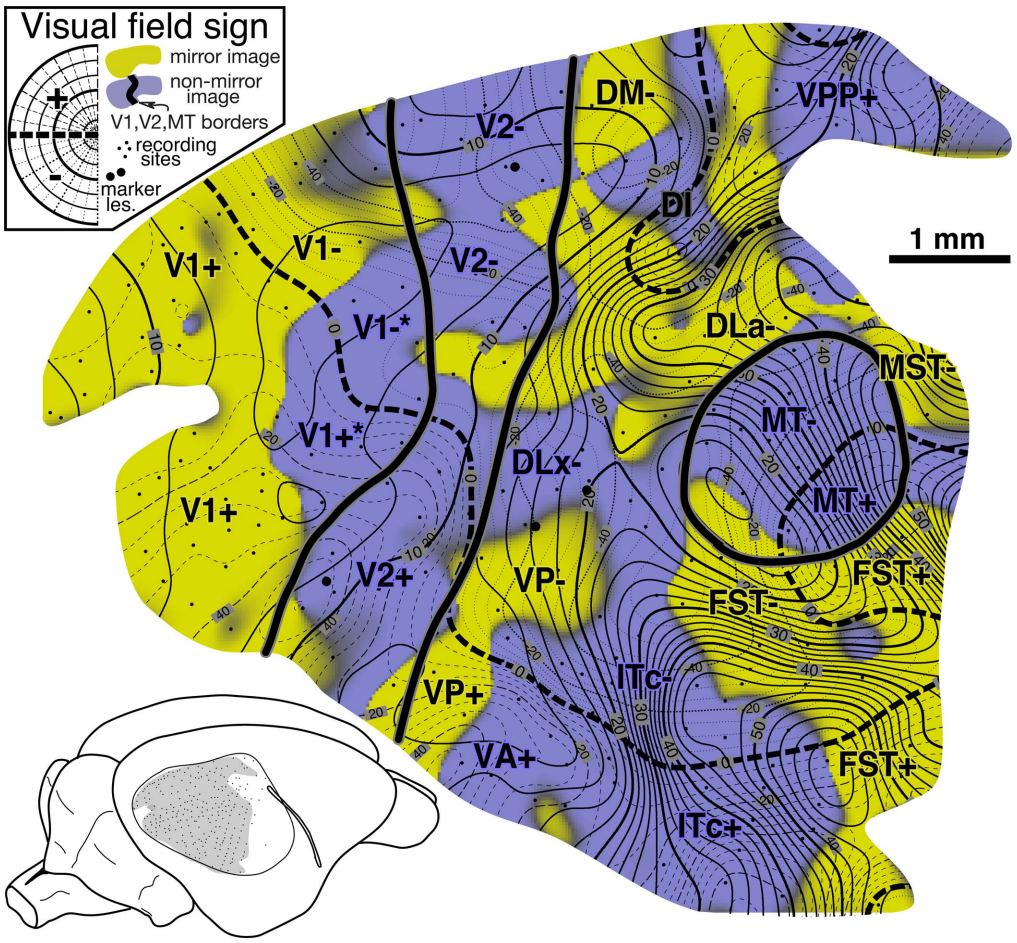

Figure 8. Double contour map with superimposed visual field sign map based on data from Figure 5. The shading now indicates the visual field sign; blue-purple is non-mirror-image (e.g., MT) and yellow is mirror-image (e.g., V1). Recording sites shown as small dots. The isoeccentricity contours are drawn in bolder solid lines to help distinguish them from the lighter, dashed isopolar angle contours. Visual field sign measures the local relation between the two contour maps, which is difficult to extract without explicit coloring. MT stands out as a squarish patch of non-mirror-image representation at the middle right. The two sets of contours there cross at right angles, indicating an approximately conformal (angle-preserving) map of the visual field. The mirror to non-mirror reversal expected at the V1/V2 border was unexpectedly displaced into the interior of architectonically-defined V1 (see Figs. 9,10). There are many local islands of differing visual field sign moving away from V2 and MT (see text). Abbreviations: V1, striate cortex; V1*, non-mirror-image striate cortex; V2, second visual area; VP, ventroposterior; DM, dorsomedial; DLa, dorsolateral anterior; DI, dorsointermediate; MST, medial superior temporal; MT, middle temporal; FST, fundus of the superior temporal sulcus area; ITc, caudal inferotemporal. The + and - indicate upper and lower visual field. The inset shows the location of the penetrations on the brain.

regions are mapped to lines of indeterminate visual field sign. A map of visual field sign is produced by distinguishing angles of 0 to π from angles of π to 2π. The local gradient directions in the r and θ maps are estimated from finite differences in r and θ in the x and y directions on the two interpolated maps. This measure is independent of position of the visual field origin, as long as the relative position of receptive fields are correct.

Figure 8 illustrates a visual field sign map calculated from the data in Figure 5. Color is now used to indicate the local visual field sign; non-mirror image (V2, MT) is blue-purple and mirror-image (V1) is yellow. Recording sites are indicated by small dots and lesions by larger dots. The interpolated contour plots from Figures 6 and 7 have also both been added to the Figure. Isoeccentricity (r) contours were drawn bolder and given larger contour annotations to help distinguish them from the lighter, dashed isopolar angle (θ) contours. The horizontal meridian is marked with a thick dashed line.

The visual field sign plot is a measure of a local relation between the two contour maps (angle between the steepest uphill directions in the two maps). One way to verify that the coloring is correct is to follow a contour in one map (e.g., one of the thicker isoeccentricity contours) while observing whether the contours that it intersects in the other map (thinner, dashed isopolar angle contours) are increasing or decreasing in value; the visual field sign coloring changes just at the point where the sequence of contours encountered in the *other* map reverse direction (i.e., go from increasing to decreasing, or *vice versa*). This well-defined local relation is, nevertheless, virtually impossible to make out given just the two contour maps without explicitly shading visual field sign.

V1 and V2. The visual field sign map in Figure 8 contains six main patches of mirror-image visual field sign (yellow) and six main patches of non-mirror-image visual field sign (blue-purpole), after discounting as artifacts a handful of small visual field sign reversals supported mainly by a single recording site. This suggests that we recorded from a minimum of 12 different visual areas in this experiment. At the far left, there is a large patch of mirror-image (yellow) representation corresponding to area V1. It is bounded on the right by a sinuous vertical band of non-mirror-image representation (blue-purple) corresponding to V2. The complexity of the boundaries of this pattern may reflect the presence of V2 stripes, which contain parallel re-representations of portions of the visual field (Rosa et al., 1988), and which have been shown with anatomical tracers to be present in another primitive primate, *Galago* (Krubitzer and Kaas, 1990). The most striking feature, however, is that the position of the mirror/non-mirror border is misaligned with the myeloarchitectonic V1/V2 border near the center of gaze (see discussion below).

VP, ITc, and FST. Toward the bottom of the map (lateral edge of the craniotomy) just anterior to V2 is a rather thin, rightward tilting vertical strip of mirror-image representation (yellow) labeled VP that contains a medial lower visual hemifield representation and a lateral upper hemifield representation. Anterior to this, in posterior inferotemporal cortex, is a large non-mirror-image patch (blue-purple) containing a representation of most of the visual field provisionally labeled ITc. It is adjoined anteriorly and above by another large patch of mirror-image representation (yellow) at the lower right labeled FST. This last patch get wider as one moves up (medially), eventually forming a broad "Y". The bottom and the right arm of the "Y" both contain upper visual field representations, while the left arm contains a lower visual field

representation. Those two upper field representations are not overlapping. The bottom of the "Y" is more eccentric than the right arm, and they could both be part of a continuous, anteriorly curving representation of the upper visual quadrant in FST, the anteriormost part of which was just beyond our exposure.

MT. Just above (medial to, on the cortex) the arms of the large mirror-image "Y" in inferotemporal cortex is a large squarish patch of non-mirror-image representation (blue-purple) with a posterior and lateral pointing center-of-gaze representation that stands out as MT. Compared to the surrounding cortex, it is particularly orderly, containing a nearly complete visual hemifield representation, and an evenly spaced, almost orthogonal set of r and θ contours, which indicate that it contains an essentially conformal (angle preserving) map of the visual field. Extending posteriorly from the upper edge of the center-of-gaze representation of MT is a small unlabeled patch of non-mirror-image representation (purple-blue) that is continuous with the center-of-gaze representation of V2. As in V1, there is a small opposite-visual-field-sign mirror-image patch (yellow) at the center of gaze of MT (see discussion below).

DLa. Just medial and posterior to MT is another strip of mirror-image representation (yellow) in the lower visual field labeled DLa. This mirror-image patch has several lobes; however, the lobe that points posterior and medially (up, between the two "V2-" annotations) is supported by very few data points (this area was less responsive than other areas). The parts of DLa nearer to MT and V2, by contrast, were more responsive, and the pattern of retinotopy better defined. The middle yellow lobe (extending directly posteriorly from the DLa- label) is supported by a number of recording sites and protrudes into V2 (see discussion below). Greater eccentricities in DLa are represented anteriorly while more negative polar angles are generally represented laterally.

DM, DI, VPP, and MST. Near the center top of the Figure, just anterior to V2 is a small mirror-image patch (yellow) labeled DM. This area contains only lower visual fields. Anterior and slightly lateral to that patch is a small non-mirror image (blue-purple) patch labeled DI that contains both upper and lower visual fields with small eccentricities situated latero-posteriorly. Just anterior to DI is an unlabeled patch of mirror image representation supported only a few points. Yet more anterior in parietal cortex is a well-supported non-mirror-image area (blue-purple) containing mostly upper visual fields that is labeled VPP+. Finally, directly anterior to MT near the border with auditory cortex, there is a small mirror-image representation (yellow) that has been labeled MST. It was supported by several strongly visually responsive points. This area was almost directly bordering auditory cortex (see Figure 2, and Figure 9 below).

Correspondence Between Visual Field Sign and Myeloarchitecture

In order to correlate the visual field sign pattern with myeloarchitecture, a single microprojector drawing made by superimposing myelin patterns from 12 sections (see Materials and Methods) was scanned, scaled, and rotated to match the visual field sign map using the marker lesions. Myeloarchitectonic borders on the scanned image at the left in Figure 9 were

then traced and superimposed as white lines on the same-sized visual field sign map at the right. The millimeter scale was measured from the cortical vasculature photograph thereby correcting for size change in the flatmounted myelin-stained sections. There detailed correspondences between the field sign map and the myelination pattern but also some unexpected divergences.

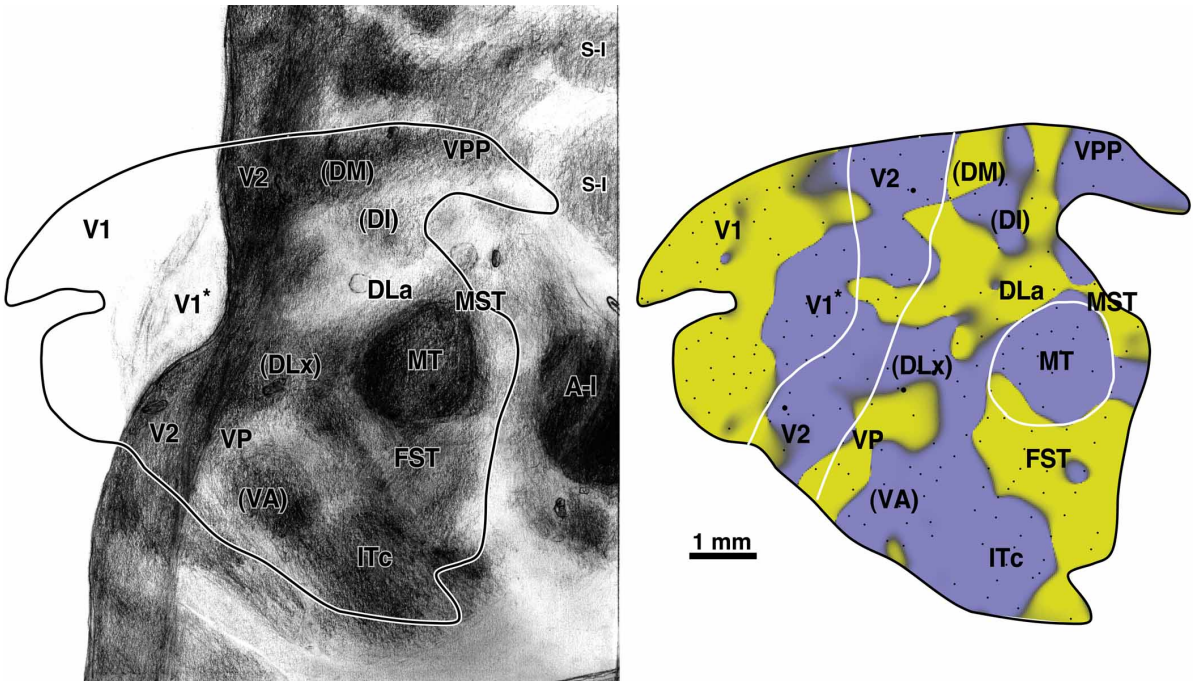

Figure 9. Correspondence between myeloarchitecture (drawing of 12 superimposed myelin-stained sections at left) and same-size visual field sign map (right). Non-mirror-image is blue-purple and mirror-image is yellow. The V1, V2, and MT myelin borders are drawn in white on the field sign map. Areal labels are in corresponding positions to facilitate comparisons. There is a good agreement on the borders of MT (except at the center of gaze, see text). There are close correspondences between myeloarchitecture and visual field sign for areas VP, ITc, FST, DLa, DM, and DI (see text). A conspicuous exception is the non-mirror-image (V2-like) patch that lies over the protruding part of myeloarchitectonic V1 (labeled V1*) where a duplication of the visual field extends over 1 mm posterior to the myeloarchitectonic V1/V2 border (see also Fig. 10). For abbreviations, see Figure 8 caption.

To aid comparisons of myeloarchitecture and visual field sign, the area labels have been placed in corresponding positions in the two maps.

Area V1. The first surprise was that the border between mirror-image representation (e.g., V1) and non-mirror-image representation (e.g., V2) deviated almost 1.5 mm into V1 as defined by myeloarchitecture near the center of gaze. This 'anomalous' non-mirror-image part of V1 (supported by many recording points) was situated in the part of myeloarchitectonically-defined V1 that protrudes anteriorly, and is labeled V1*. Figure 10 shows receptive field charts from two penetration rows across the V1 border. In the top (medial) penetration row, receptive fields reached the vertical meridian just as the penetrations passed into myeloarchitectonically defined V2, where the visual field sign reversed as expected. In the bottom row, however, receptive fields

reached the vertical meridian *within* myeloarchitectonically-defined V1 but then turned away from the vertical meridian while still inside V1, resulting in a non-mirror-image (V2-like) visual

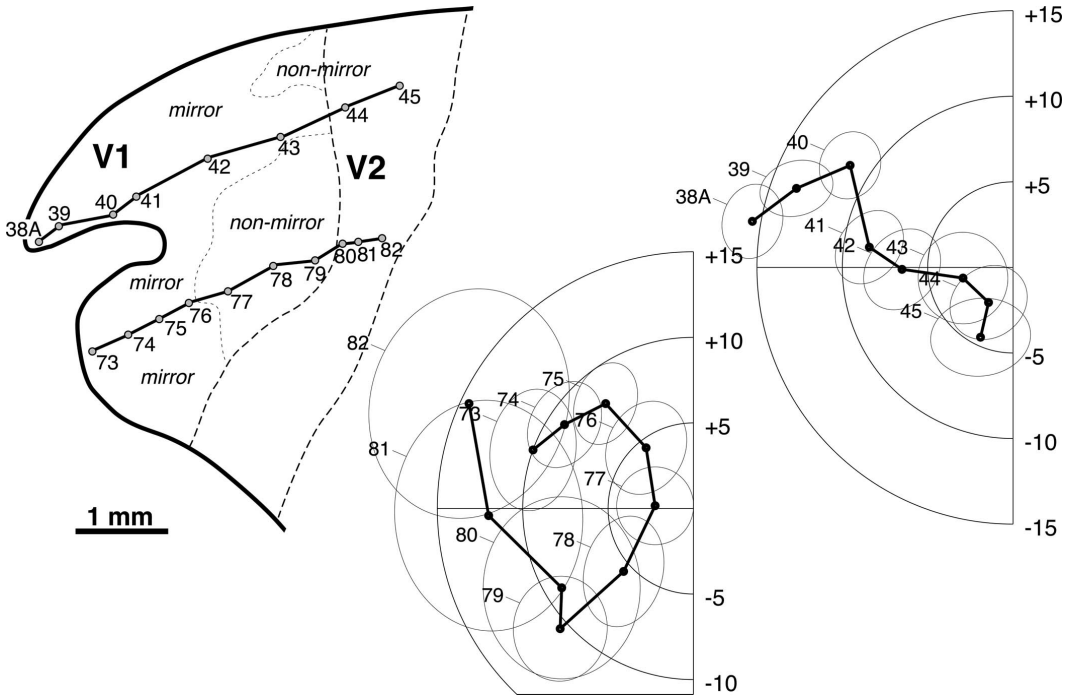

Figure 10. Receptive field charts from two penetration rows across the myeloarchitectonic V1 border. In the top penetration row (receptive fields in top right plot), receptive fields reached the vertical meridian and turned back as the row progressed into myeloarchitectonically defined V2. In the bottom penetration row (receptive fields in middle plot), by contrast, the receptive fields reached the vertical meridian *within* myeloarchitectonically-defined V1 and then turned away from the vertical meridian as they entered cortex containing a non-mirror-image (V2-like) duplication of the visual field. Receptive field size did not increase, however, until the penetrations reached architectonically defined V2. The early parts of both rows show a tendency for more lateral recording sites to generate receptive fields further into the upper visual field, as expected in V1. However, this relation breaks down in the anomalous non-mirror-image part of myeloarchitectonic V1.

field representation. Notably, receptive field size did *not* increase, however, until the penetrations reached architectonically defined V2 (receptive fields 79 to 80).

MT, DLa, FST. The borders of MT, as defined independently by a region of heavy myelination and a patch of non-mirror-image visual field sign showed a striking correspondence -- agreeing for the most part to within ±50 μm of each other. There was a clear discrepancy, however, again at the center of gaze representation, where a 300 μm wide patch of reversed (mirror-image in this case) visual field sign appeared. This interestingly recalls the reversed visual field sign patch in central V1 in the same animal. Four rows of penetrations through MT (non-mirror image part) and their corresponding receptive fields are illustrated in Figure 11. The receptive field rows throughout MT are rigorously parallel, indicating that the visual field representation is orderly. The visual areas surrounding MT -- the lower quadrant map in DLa and

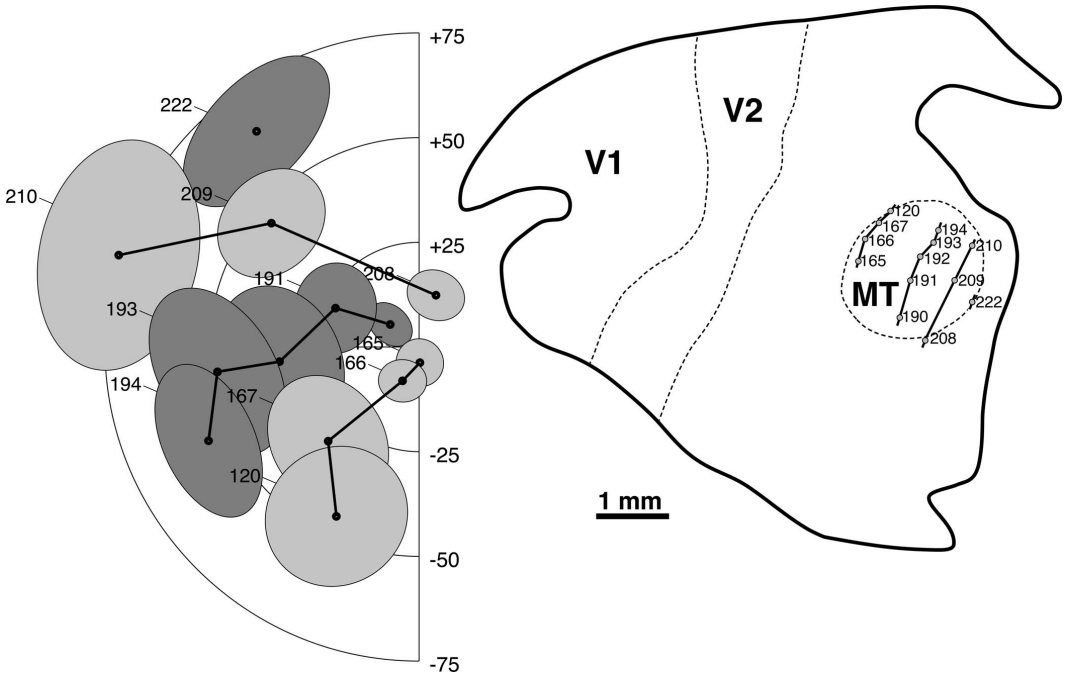

Figure 11. MT receptive fields. Four rows of penetrations (the last 'row' containing a single penetration) are illustrated at the right. The dashed lines illustrate the position of the myeloarchitectonically defined V1, V2, and MT. The corresponding receptive field sequences from these rows are shown in alternating grays. The sequences are well behaved (approximately parallel with none crossing) indicating that the MT visual field representation is orderly, which is confirmed by the evenly-spaced, orthogonal r and θ contours visible in MT in Figure 8. Note that the maximum eccentricity on the receptive field chart is three times that in the previous Figure.

the nearly full-hemifield map in FST -- were nearly as well-organized as MT (see Fig. 12), and corresponded closely with a lightly myelinated strip (DLa) and a medium-density myelinated triangle (FST).

Area V2. The myeloarchitectonic boundaries of V2 contained mostly non-mirror image field sign as expected. However, there was a prominent finger of mirror-image fieldsign (yellow, its posterior end is near the V1* label in Figure 9) within architectonic V2. One possibility is that this is a re-representation of the visual field due to the V2 stripes. However, the reversed visual field sign intrusion is in a roughly similar to the location of the duplicated visual field in V1 (see Discussion).

Close examination shows a number of peculiarly detailed correspondences between visual field sign and the myelin pattern. The mirror-image finger in V2 discussed above, for example, is more lightly myelinated than surrounding V2. And just medial (up) from the 'anomalous' V2 mirror-image (yellow) 'finger' is a small anteriorly protruding patch of non-mirror-image representation (blue-purple) that corresponds closely to a small myelinated oval just beyond the marked anterior border of V2. Finally, in between the center of gaze representation of V1/V2 and MT just below DLa is a small patch of non-mirror-image representation (blue-purple) that lies almost exactly over a slightly larger, moderately-myelinated strip (labeled DLx in Fig. 9).

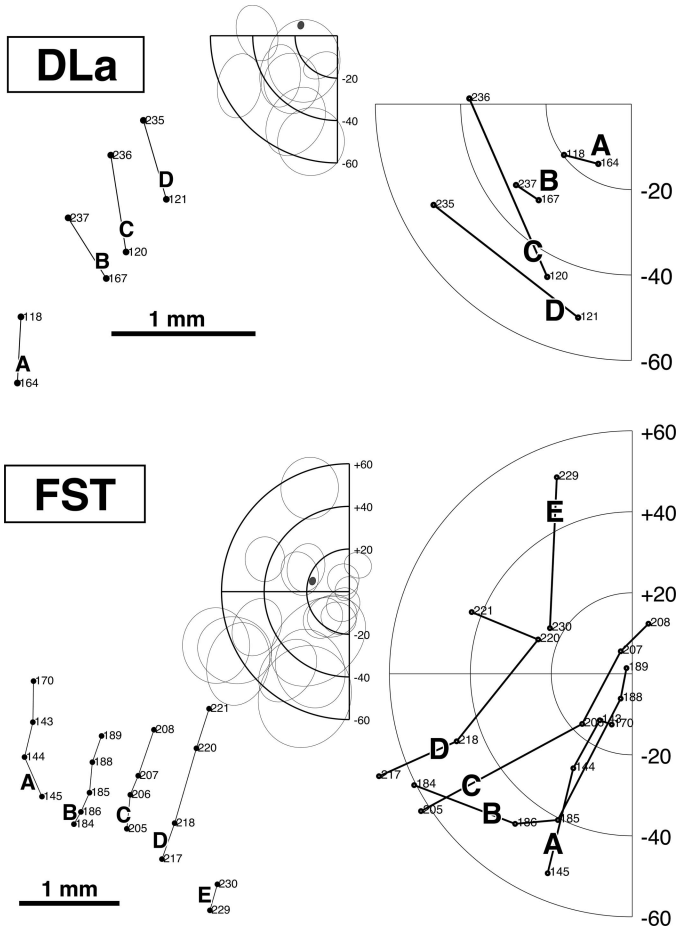

Figure 12. Orderly visual field representations from DLa and FST. Penetration maps are at the left, receptive field coverage in the middle, and receptive field center sequences at the right.

Many of the other visual field sign regions described previously in Figure 8 show close correlations with the myelin pattern. The laterally located mirror-image (yellow) strip labeled VP that is just anterior to V2 corresponds closely to a lightly myelinated strip just anterior to myeloarchitectonic V2; and the most medial extent of this region bends anteriorly in both fieldsign and myelin view. The large non-mirror-image patch (blue-purple) in posterior inferotemporal cortex, labeled (VA) and ITc, corresponds quite closely to two large myelinated patches. The correspondence extends even to the presence of a small dent in both the visual field sign and myelin patterns (just above the "ITc" label). Most of the Y-shaped mirror-image (yellow) patch labeled FST at the lower right corresponds to the patch of medium-dense myelination (less dense than ITc).

Near the medial (up) edge of the exposure, just anterior to V2, there are two densely myelinated anterior-posterior strips; one is just inside the exposure and one medial to it. The mirror-image (yellow) strip labeled DM near the medial border of the craniotomy just anterior to V2 corresponds to the posterior half of the more lateral myelinated strip. The non-mirror image patch of DI (blue-purple) corresponds a small region of intermediate myelination lateral to DM.

The anteriorly located non-mirror image patch (blue-purple) labeled VPP corresponds with the anterior part of the lateral myelinated strip. Finally, MST as defined by mirror-image (yellow) visual field sign corresponds to some degree with a thin myelinated strip adjoining MT anterio-medially.

Discussion

Multiple retinotopically organized visual field maps characterize the tangential organization of most of the visual half of neocortex in primates (review: Sereno and Allman, 1991; Sereno and Tootell, 2005; Huang and Sereno, 2018). Areas have typically been individuated by converging lines of evidence including visuotopic organization, architectonic features, connection patterns, and physiological properties. In monkeys, for example, MT contains relatively undistorted map of the entire contralateral visual hemifield. The electrophysiologically defined borders of the MT map coincide quite closely with a clear architectonic feature (heavy myelination in lower cortical layers in MT), a connectional feature (MT receives V1, layer 4B input), and a physiological feature (most MT cells are direction selective). Unfortunately, few other areas are as clearly defined as MT.

In the present work on a representative of a little-studied group of primates that retain features of the earliest primates, we have concentrated on retinotopic features of cortical areas analyzed by visual field sign to aid in defining areal boundaries. We then correlated visual field sign with architectonic features visible in a flatmount of the same cortex stained for myelin. We have definitive evidence for the existence of MT. We also obtained evidence for a large number of additional areas, most of which have reasonably obvious analogues with visual areas in other primates. Surprisingly, we uncovered a curious inversion of visual field sign at the center of gaze, indicating a small visual field duplication entirely within the borders of architectonically defined V1.

Using Visual Field Sign to Define Cortical Areas

Visual field sign (non-mirror-image vs. mirror image visual field representation) is a locally-defined property of visual cortex that can be used alongside myeloarchitectonic, cytoarchitectonic, connectional, and physiological criteria to parcellate visual cortex. It was developed out of necessity in dealing with large retinotopic mapping data sets as a helpful first-pass analysis. The standard technique of picking subsets of receptive fields and corresponding penetration charts is useful to argue for a particular subdivision of the data, after subdivision has been achieved. But it is less suited to deciding how to divide up large data sets in the first place because there are so many possible subsets of, say, ten receptive fields, out of several hundred recording sites to consider. Also, visual field sign makes use of all of the available mapping data and reduces the temptation to discount or ignore 'anomalous' data points; by first calculating visual field sign, an objective subdivision of the data based *only* on retinotopy can be compared with completely independently derived evidence on myeloarchitectonic features.

It's worth keeping in mind that visual fieldsign is only one feature among several. Thus, if a other features suggest that two regions with *opposite* visual fieldsign are similar, one could argue that they nevertheless belong to a single area. For example, Yu et al. (2020) argue that marmoset DM is just such a case where the constraints of maintaining congruent borders with other visual areas may actually disrupt the continuity of visual fieldsign within DM (at the cost of an internal incongruent border). Conversely, there may be reasons to distinguish adjoining regions of the cortex with the *same* visual field sign -- just as we might distinguish areas that share similar patterns of myelination or similar receptive field size -- if there are other criteria on which those areas sharply differ (see e.g., lower field V2 and adjoining upper field DI in owl monkeys, both non-mirror-image representations in Sereno et al., 2015).

Visual Field Sign is Invariant to Receptive Field Coordinate Transformations

An important feature of the visual field sign measure is that it is invariant to transformations of the coordinate system in which the receptive fields were digitized. For example, if one were to redefine the receptive field chart coordinate system so that all the receptive fields were displaced 10 degrees peripherally along the horizontal meridian, and then all rotated rigidly 5 degrees in a clockwise direction, the visual field sign map calculated from the transformed set of receptive fields would be unchanged, despite the fact that every contour in the r and θ maps would have changed position.

This frees us from relying heavily on the absolute values of r (eccentricity) and θ (polar angle) for defining areal boundaries. Areal boundaries often fall near the ideal vertical and horizontal meridians. Nevertheless, 'real' vertical and horizontal meridians -- even those of V1 and V2 -- are typically somewhat undulatory in the visual field, and difficult to define objectively (see discussion in Sereno et al., 2015). A relative measure like visual field sign will accurately find borders not only in those cases, but also in cases where the border between areas occurs at a substantial distance from either the vertical or horizontal meridian. This last condition appears to be a common occurrence in extrastriate cortex (see e.g., Gattass et al., 1988; Neuenschwander et al., 1994; Sereno et al., 1994); it will vitiate a search for areal boundaries based on particular values of r and θ.

Visual Field Sign Reversal Within Myeloarchitectonically-defined V1

One of the most surprising results was that there appeared to be a reversal in visual field sign contained entirely within the borders of myeloarchitectonically-defined V1, indicating a localized duplication of the visual field. This is such an unexpected result that it needs to be confirmed in additional animals. We are extremely confident that this was not an eye drift artifact since we repeatedly checked the projection of multiple retinal landmarks onto the hemisphere and they were completely stable for the entire duration of the experiment. The anomalous receptive fields were 5-10 degrees away from their expected positions -- well beyond any possible error in back projection. This specific region of the cortex is challenging to explore electrophysiologically in monkeys because of its inaccessibility at the lateral convexity of cortex,

but also because receptive fields there are so small and magnification factor so great near the center of gaze in diurnal primates that it is much more difficult to make out receptive field sequences than it is in galagos or lemurs. Those considerations also makes it challenging to determine visual field sign there from classical 2-DG or fMRI experiments. It's worth noting that such an unusual organization has not previously been mooted.

The 'anomalous' part of V1 corresponds with a characteristic promontory in the myeloarchitectonic V1/V2 border visible in flatmounted cortex. A similar feature is visible in the flatmounted cortices of many other primates including galagos (personal observations), owl monkeys (Tootell et al., 1985; Sereno et al., 1994), squirrel monkeys (Livingstone and Hubel, 1984), and macaques (Van Essen et al., 1986).

In *Galago senegalensis*, there is a small area with an almost complete visual field representation directly adjoining the V1 border just lateral to the center of gaze that displaces V2 to either side (Allman and McGuinness, 1983). The lateral and posterior limits of our exposure barely prevented us from reaching the corresponding area in the present experiment. Nevertheless, that area in galagos provides additional evidence for hitherto unsuspected complexity in and around the V1/V2 center-of-gaze representation in some primates.

A partial map duplication in a primary sensory area is not unprecedented. For example, in somatosensory area S-I of the grey squirrel, Sur et al. (1978) found a duplication of just the hand and parts of the forearm embedded within a single coherent representation of other parts of the body (hemi)surface.

Area MT

One of the clear-cut results of this study was the confirmation of a classical MT in this species. This area's position (between the center of gaze of V1 and primary auditory cortex nearer the latter), orientation (center of gaze points ventroposteriorly), shape (elliptical), visual field sign (non-mirror-image), visual topography (complete hemifield without major discontinuities), myeloarchitecture (densely myelinated, especially in lower cortical layers), and response properties (brisk, direction-selective) all point to its identity as MT. The correlation between the borders of MT independently derived from the visual field sign calculation and from the pattern of myelination was remarkably exact given the moderate number of penetrations we were able to place into this small area.

A prominent elliptical MT thus appears to be a primitive features for primates -- that is, all primates seem to have retained such an area, which probably arose in its present form very early in primate evolution. Despite the small size of the cortex of *Cheirogaleus* (somewhat smaller in area, for example, than the cortex of a California ground squirrel with a comparable body size) the disposition of V1 and MT gives it the unmistakable appearance of the cortex of a primate.

Intriguingly, an 'anomalous' reversed field sign region similar to that found in V1 (here, mirror-image (yellow) within otherwise non-mirror-image MT) was found at the center of gaze of MT, consistent with the results in V1.

Multiple Areas in Between V2 and MT

Most of the cortex directly between V2 and MT contains representations of the lower visual field. The more dorsal part of this region has been divided up into several distinct areas in monkeys -- DLp, DLi, and DLa in owl monkeys and V3A, V4, and V4t in macaque monkeys (Sereno and Allman, 1991; Felleman and Van Essen, 1991). In *Cheirogaleus*, there is a well-organized DLa in contact with MT. However, the cortex posterior to DLa and MT is organized differently than in New World Monkeys. There is no obvious DLi (only tiny fragments of non-mirror-image cortex protruding anterio-medially, halfway between the "DLx" and DLa" labels in Fig. 8). Posterior to that, there is an unlabeled, mirror-image region (yellow) that could be similar to owl monkey DLp, but it doesn't continue laterally, where the field sign reverses to non-mirror-image in a region temporarily labeled DLx.

The retinotopic organization of this region of the cortex appears to be somewhat unstable and quite variable across several primates, even among conspecific individuals (see discussion in Sereno et al., 2015; Angelucci and Rosa, 2015). Our penetration density was constrained by the need to cover a reasonable area, but could have been too low here; for example, tangential penetrations through cortex surrounding MT in *Galago* revealed a well-organized lower visual quadrant representation packed into thin strip only half a millimeter wide (Allman and McGuinness, 1983).

Moving medially, as in both New and Old World monkeys (DI, V3A), there appears to be a small finger of non-mirror-image *upper* visual field representation that protrudes downward into the region between V2 and MT. This upper field representation lies within a moderately myelinated zone just lateral to area DM and resembles the area originally labeled DI in owl monkeys, but doesn't quite touch V2 as DI does in New World monkeys (Sereno et al., 2015, Fig. 2). There is connectional evidence for upper fields here in galagos (Fig. 3 from Kaskan and Kaas, 2007).

Other Parietal and Temporal Areas

We found a mirror-image area, the dorsomedial area, DM, directly adjoining V2 dorsally that is heavily myelinated (Allman et al., 1979, and Krubitzer and Kaas, 1993, Rosa and Schmid, 1995; Wong and Kaas, 2010). Recent optical imaging data from galagos (Fan et al., 2012) from a smaller recording region centered slightly medial to ours found a lower field region in the location of our DM-, which they labeled V3-. Our polar angle map (Fig. 7) certainly shows lower visual fields anterior to V2- in the location of the optical recordings. However, note that moving laterally, there are reversals in polar angle that are inconsistent with a continuous, V2-like V3. A lateral-to-medial traverse in Figure 7, half a mm anterior to the V2 border, starting from VP+ reveals: upper (red), horizontal meridian (blue), lower (green), horizontal meridian (blue), lower (green), horizontal meridian (blue).

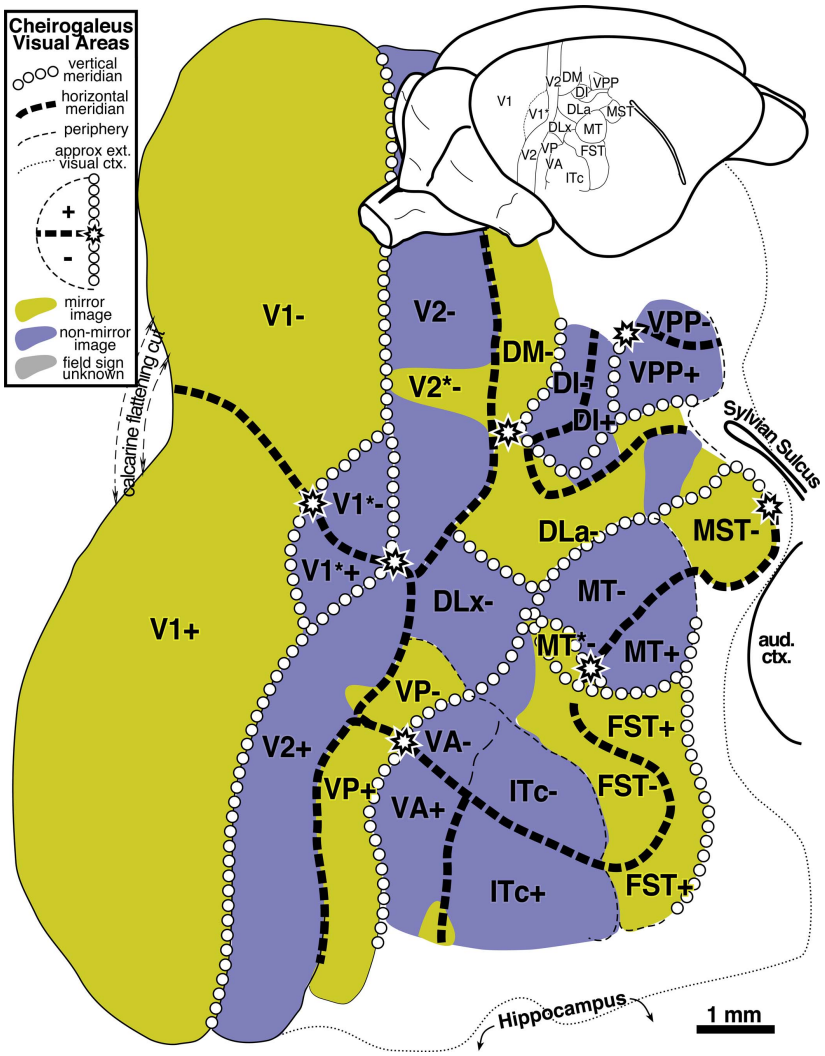

Figure 13. Summary diagram of the retinotopic organization of lateral extrastriate visual areas in the fat-tailed dwarf lemur, *Cheirogaleus medius,* drawn using the myelin-stained right hemisphere as a template. The horizontal meridian is indicated by a thick dashed line, the vertical meridian (both upper and lower) by rows of small circles, the periphery by a thin dashed line, and the center of gaze by a star (see upper left inset). The thin dotted line shows the estimated outer boundary of visual cortex. Since many transitions between areas do not occur exactly at the vertical or horizontal meridians, this diagram should be treated as an easier-to-read caricature of the actual retinotopic map shown in Figure 8. The upper right inset shows the position of the named areas on the brain.

Anterior to DM and DI, there is a well-organized non-mirror image region VPP with large receptive fields that contains lateral upper visual fields and medial lower visual fields, as in owl monkeys.

Directly anterior to MT is a mirror image area, MST whose position and visual field map orientation and sign closely resembles owl monkey MSTd.

Moving laterally and posteriorly, we found a mirror-image (yellow) ventral area, VP, directly anterior to ventral V2 containing an upper visual field representation but also a small, continuous, more dorsally located lower visual field representation, closely resembling the

situation in several New World monkeys (see detailed discussion in Sereno et al., 2015; Jeffs et al., 2015; Angelucci et al., 2015; Angelucci and Rosa, 2015).

Anterior to VP, there was a large patch of non-mirror-image cortex (blue-purple), with a tiny finger of mirror image cortex protruding into it from the lateral edge. The polar angle map (Fig. 7) shows systematic, alternating upper field vertical meridians (red) and horizontal meridians (blue) that would seem to resemble the situation in owl monkeys -- in order, by color: red V1/V2 border, blue V2/VP border, red VP/VA border, blue VA/ITc border). However, in contrast to owl monkeys, ITc is very clearly non-mirror-image (blue-purple), not mirror-image (yellow).

Finally anterolateral to MT is a well-organized mirror-image FST. Like ITc, FST contains a retinotopically well-organized representation of both lower and upper visual fields. FST as defined here shares its center-of-gaze representation with MT. At a result of its curvature, FST shares its periphery with ITc. We have retained the term FST derived from research in other primates although the superior temporal sulcus is not present in *Cheirogaleus*.

***Summary Map for Visual Areas in* Cheirogaleus**

Figure 13 shows a schematic diagram of the retinotopic organization of visual areas in *Cheirogaleus* drawn using the myelin-stained flatmounted right hemisphere as a template, using standard conventions for the vertical meridians (circles) and horizontal meridians (thick dashes) meridians. These notations have been used rather loosely, as is the custom in the literature, to indicate the general orientation and visual field sign of a retinotopic patch rather than as substitutes for the actual retinotopic contours illustrated in Figures 6-8. In many cases, re-representations of the visual field are incomplete, containing only one quadrant or just a portion of both quadrants. Restriction of the vertical and horizontal meridian, center-of-gaze, and periphery symbols to these exact locations would eliminate many of these symbols from this diagram (as well as from similar diagrams presented by other laboratories). There are 21 distinguishably different representations of the upper and lower visual hemifields. Overall, there is a considerable degree of similarity to organization of retinotopic maps constructed for other primates.

***Phylogenetic Position of* Cheirogaleus**

The phylogenetic relationships of primitive primate species -- particularly fossil species -- has been contentious (for reviews see: Szalay and Delson, 1979; Fleagle, 1988; Martin, 1993). One difficulty is the sparseness of the fossil record. There are currently about 200 living primate species. Even with conservative assumptions about the survival time of individual species and the time of origin of primates, it is likely that thousands of primate species preceded the ones that exist today (Martin, 1993). Set against this large number are the 250 species of fossil primates that have been recognized to date (Szalay and Delson, 1979). Another recurrent problem has been the tendency to conflate the polarity of change in a character (the distinction between a primitive and a derived feature) with relative position in a phylogenetic sequence (position in a branching pattern). The various features of an organism can and do evolve independently from

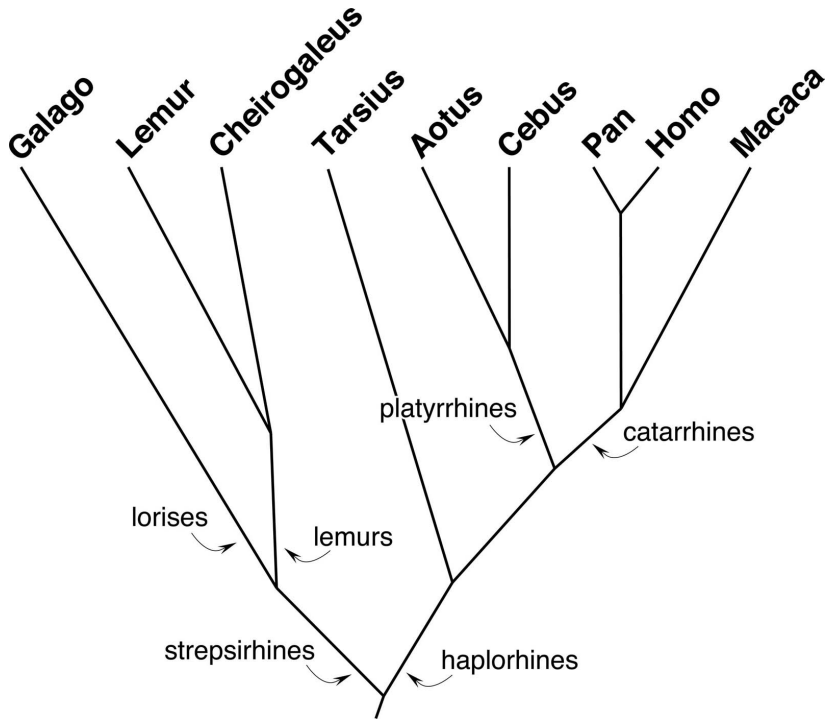

Figure 14. Phylogenetic relationships of familiar representatives of living primate groups with branch points drawn along the y-axis to indicate estimated relative times of divergence (based on Koop et al., 1989; Duffy et al., 1990; Martin, 1990; 1993). The deepest branch in the tree (strepsirhine/haplorhine) has been dated to at least 65 Myr ago while the most recent (chimp/human) is though to have occurred ~5 Myr ago. The fat-tailed dwarf lemur, *Cheirogaleus medius*, has been grouped with the other Madagascar lemurs as opposed to lorises (see text). Area MT has been positively identified in *Galago*, *Cheirogaleus*, *Lemur* (personal observations), *Aotus*, *Macaca*, *Pan*, and *Homo*, suggesting that MT is a primitive character for all primates that achieved its characteristic form in an early nocturnal primate.

each other, making it very unlikely that there are any species characterized only by primitive features. A 'primitive' species in a group (e.g., the platypus in the case of mammals) at a great phylogenetic distance from a more 'advanced' species (e.g., a placental carnivore like a cat), nevertheless has many derived features (e.g., the platypus bill and electric sense (Scheich et al., 1986; Pettigrew, 1999)) that distinguish it from the last common ancestor of the two species. Thus, it is very unlikely that the earliest mammals were characterized by a platypus-like bill and an electric sense. Conversely, an 'advanced' species may have retained many generalized, primitive features. For the present purposes, these considerations should strongly caution us against assuming that the cortical organization of any living primitive primate species has remained unchanged from that of the early ancestors of primates.

Cheirogaleus medius, the fat-tailed dwarf lemur and *Microcebus murinus*, the mouse lemur (Nadkarni et al., 2019), had traditionally been thought to be most closely related to other Malagasy lemurids (e.g., *Lemur, Indri, Daubentonia*), perhaps as the most primitive species of that group. The Malagasy lemurid group together with the African/Asian lorisids (e.g., *Galago*, *Loris*, *Nycticebus*) form the primate suborder Strepsirhini (initially named for a primitive retention -- a cleft in the upper lip region -- but now usually united by the shared derived features

of a dental tooth comb and a grooming claw on the second toe). Charles-Dominique and Martin (1970), however, noting similarities between the pattern of cerebral blood circulation in cheirogaleids and lorisids, removed cheirogaleids from the Malagasy lemurid group and grouped them instead with lorisids (see also Szalay and Delson, 1979; Schwartz, 1986; Yoder, 1992). Recent molecular evidence (blood protein sequences), nevertheless, has reaffirmed the more traditional view that cheirogaleids should be grouped first with the lemurids (Koop et al., 1989; Duffy et al., 1990). In Figure 14, we have summarized the branching pattern primates using well-studied representatives of each major group. The position of *Cheirogaleus* is based on the molecular evidence. Two main fossil primate groups of uncertain affinities (Martin, 1993) -- the adapids and omomyids -- have been omitted.

Galago is the only other strepsirhine primate whose visual cortex has been examined by detailed retinotopic mapping (Allman et al., 1973; Allman et al., 1979; Allman and McGuinness, 1983; Fan et al., 2012). Given that *Cheirogaleus* and all other primates so far examined have a clear area MT, we think it is quite likely that MT is a primitive feature for all primate groups. As in the case of cytochrome oxidase blobs, it appears that the characteristic form of primate MT was attained in small nocturnal primates, and then primitively retained as color vision and diurnal habits were acquired by monkeys and apes. More broadly, the presence of an extensive array of cortical visual areas in *Cheirogaleus* that can be reasonably homologized with those reported from other primates suggests the extensive array is itself a primitive feature within the primate order (Allman, 1977), which would be consistent with a large occipital-temporal area present in endocasts of primates of the early Eocene such as *Tetonius* (Radinsky, 1967).

Some Outgroup Comparisons

MT-like areas. Several other mammals have a myelinated, cytochrome oxidase-rich area situated in between V1 and auditory cortex; it is separated from V1 by several additional areas, and from auditory cortex by a very lightly myelinated strip as it is in primates (e.g., TP in squirrels: Paolini and Sereno, 1998; PMLS in cats: Olavarria and Van Sluyters, 1985; lateral myelinated zone in flying foxes: Rosa et al., 1993, their Fig. 9). But there are a number of physiological, connectional, and retinotopic features of these other areas that differ from those of MT. In squirrels, for example, the lateral myelinated, cytochrome oxidase rich area TP does not receive a direct input from V1 (Kaas et al., 1989) and contains very large receptive fields that are *not* direction-selective (Paolini and Sereno, 1998), while in cats, V1-recipient area PMLS (whose anterior portion contains a non-mirror-image representation like MT, but with the center of gaze oriented anteriorly, in contrast to MT: Palmer et al., 1978) also receives a strong direct input from W-like cells in the C laminae of the lateral geniculate nucleus (Rosenquist, 1985).

DM/V3-like areas. If we countenance the possibility of a DM containing not only mirror-image but also non-mirror-image maps (Rosa and Schmid, 1995; Yu et al., 2020), we might be tempted to join the slightly discontinuous, more anterior upper field patch (here labeled DI+)

with our DM-. However, the resulting neighbor relations are different from both marmosets and owl monkeys, where upper fields directly touch lower field V2.

Inferotemporal Cortex. It is not currently clear what the large posterior inferotemporal area in *Cheirogaleus* corresponds to in monkeys. Posterior inferotemporal cortex in monkeys (e.g., Boussaoud et al, 1990; 1991; Sereno et al., 2015) is retinotopically organized. This area in *Cheirogaleus* shows a particularly clear retinotopic organization; but unlike monkeys, it contains a representation of a much larger range of eccentricities, extending out to 60 degrees eccentricity. In this respect, it is quite similar to posterior and intermediate inferotemporal cortex in galagos (Allman and McGuinness, 1983, and unpublished observations), which is also retinotopically organized, and which also contains an extensive representation of the periphery. We did not have access to the anteriormost extent of inferotemporal cortex in the present experiment; inferotemporal cortex extends far ventrally in this animal due to the almost vertical orientation of the Sylvian sulcus. Recordings from that region could determine whether a nontopographically organized anterior inferotemporal cortex is -- like MT-- a shared primitive feature for all primates, or whether anterior inferotemporal cortex was initially entirely retinotopic and only later evolved non-retinotopic intermediate and anterior regions in monkeys (Felleman et al., 1986). A geographically similar region of the cortex of the cat (Tusa and Palmer, 1980; Updyke, 1986) and the California ground squirrel (Paolini and Sereno, 1998) is retinotopically organized.

Notes

We thank Miriam Rusch and Janet Baer for veterinary assistance with the animal. We also thank Laura Korobkova and Ryan Cabeen for digitizing and assembling the high resolution photomontage of the recorded hemisphere and the retina.

Figure Captions

Figure 1. embedded
Figure 2. embedded
Figure 3. embedded
Figure 4. embedded
Figure 5. embedded
Figure 6. embedded
Figure 7. embedded
Figure 8. embedded
Figure 9. embedded
Figure 10. embedded
Figure 11. embedded
Figure 12. embedded
Figure 13. embedded

Figure 14. embedded

References

Allman, J.M. (1977) Evolution of the visual system in the early primates. *Progress in Psychobiology and Physiological Psychology* **7**:1-53.

Allman, J.M. and J.H. Kaas (1971) The representation of the visual field in the caudal third of the middle temporal gyrus of the owl monkey (*Aotus trivirgatus*). *Brain Research* **31**:85-105.

Allman, J.M. and J.H. Kaas (1974) A crescent-shaped area surrounding the middle temporal area (MT) in the owl monkey (*Aotus trivirgatus*). *Brain Research* **81**:199-213.

Allman, J.M., J.H. Kaas, and R.H. Lane (1973) The middle temporal visual area (MT) in the bushbaby, *Galago senegalensis*. *Brain Research* **57**:197-202.

Allman, J.M. C.B.G. Campbell, and E. McGuinness (1979) The dorsal third tier area in *Galago senegalensis*. *Brain Research* **179**:355-361.

Allman, J.M. amd E. McGuinness (1983) The organization of cortical visual areas in a strepsirhine primate, *Galago senegalensis*. *Society for Neuroscience, Abstracts* **9**:957.

Anderson, P.A., J. Olavarria, and R.C. Van Sluyters (1988) The overall pattern of ocular dominance bands in cat visual cortex. *Journal of Neuroscience* **8**:2183-2200.

Angelucci, A., A.W. Roe, and M.I. Sereno (2015) Controversial issues in visual cortex mapping: Extrastriate cortex between areas V2 and MT in human and nonhuman primates. *Visual Neuroscience* 32:e025, 3 pages.

Angelucci, A., and M. Rosa, M. (2015). Resolving the organization of the third tier visual cortex in primates: A hypothesis-based approach. *Visual Neuroscience*, **32**:e010, 26 pages.

Boussaoud, D., L.G. Ungerleider, and R. Desimone (1990) Pathway for motion analysis: cortical connections of visual areas MST and FST in the macaque. *Journal of Comparative Neurology* **296**:462-495.

Boussaoud, D, R. Desimone, and L.G. Ungerleider (1991) Visual topography of area TEO in the macaque. *Journal of Comparative Neurology* **306**:554-775.

Charles-Dominique, P. and R.D. Martin (1970) Evolution of lemurs and lorises. *Nature* **227**:257-260.

Desimone, R. and L.G. Ungerleider (1986) Multiple visual areas in the caudal superior temporal sulcus of the macaque. *Journal of Comparative Neurology* **248**:164-189.

Duffy, L.K., J. Luick, and D.H. Coppenhaver (1990) Prosimian hemoglobins -- V. The primary structure of the α-I, α-II and β-hemoglobin chains of *Hapalemur griseus*, with a note on the classification of *Microcebus*. *Comparative Biochemistry and Physiology B* **97**:261-267.

Fan, R.H., M.K.L. Baldwin, W.J. Jermakowicz, V.A. Casagrande, J.H. Kaas, and A. W. Roe (2012) Intrinsic Signal Optical Imaging Evidence for Dorsal V3 in the Prosimian Galago (Otolemur garnettii). *Journal of Comparative Neurology* **520**:4254-4274.

Fleagle, J.G. (1988) *Primate Adaptation and Evolution*. Academic Press.

Fiorani, M., R. Gattass, M.G.P. Rosa, and A.P.B. Sousa (1989) Visual area MT in the *Cebus* monkey: location, visuotopic organization, and variability. *Journal of Comparative Neurology* **287**:98-118.

Felleman, D.J., J.J. Knierim, and D.C. Van Essen (1986) Multiple topographic and non-topographic subdivisions of the temporal lobe revealed by the connections of area V4 in macaques. *Society for Neuroscience, Abstracts* **12**:1182.

Felleman, D. and D.C. Van Essen (1991) Distributed hierarchical processing in primate visual cortex. *Cerebral Cortex* **1**:1-47.

Gallyas, R. (1979) Silver staining of myelin by means of physical development. *Neurological Research* **1**:203-209.

Gattas, R., A.P.B. Sousa, and C.G. Gross (1988) Visuotopic organization and extent of V3 and V4 of the macaque. *Journal of Neuroscience* **8**:1831-1845.

Huang, R.-S. and M.I. Sereno (2018) Chapter 7. Multisensory and Sensorimotor Maps. In: *The Parietal Lobe. Neurological and Neuropsychological Deficits* (Handbook of Clinical Neurology), G. Vallar, H.B. Coslett (eds.), volume 151 (3rd series), Elsevier, pp. 141-161.

Hubel, D.H. and M.S. Livingstone (1988) Segregation of form, color, movement, and depth: anatomy, physiology, and perception. *Science* **240**:740-749.

Jeffs, J., F. Federer, and A. Angelucci (2015) Corticocortical connection patterns reveal two distinct visual cortical areas bordering dorsal V2 in marmoset monkey. *Visual Neuroscience* **32**: e012, 24 pages.

Kaas, J.H., L.A. Krubitzer, and K.L. Johanson (1989) Cortical connections of areas 17 (V1) and 18 (V2) of squirrels. *Journal of Comparative Neurology* **281**:426-446.

Kaas, J.H., and L.A. Krubitzer (1991) The organization of extrastriate visual cortex. In B. Dreher and S.R. Robinson (eds.), *Neuroanatomy of Visual Pathways and their Retinotopic Organization*, Vol 3, Vision and Visual Dysfunction. J. Cronly-Dillon (gen. ed.). London: Macmillan, pp. 302-359.

Kaas, J.H., and A. Morel (1993) Connections of visual areas of the upper temporal lobe of owl monkey: the MT crescent and dorsal and ventral subdivisions of FST. *Journal of Neuroscience* **13**:534-546.

Kaskan, P. and J.H. Kaas (2007) Cortical connections of the middle temporal and middle temporal crescent visual areas in prosimian galagos (*Otolemur garnetti*). *The Anatomical Record* **290**:349-366.

Koop, B.F., D.A. Tagle, M. Goodman, and J.L. Slightom (1989) A molecular view of primate phylogeny and important systematic and evolutionary questions. *Molecular Biology and Evolution* **6**:580-612.

Krubitzer, L.A. and J.H. Kaas (1990) Cortical connections of MT in four species of primates: areal, modular, and retinotopic patterns. *Visual Neuroscience* **5**:165-204.

Krubitzer, L.A. and J.H. Kaas (1993) The dorsomedial visual area of owl monkeys: connections, myeloarchitecture, and homologies in other primates. *Journal of Comparative Neurology* **334**:497-528.

Livingstone, M.S. and D.H. Hubel (1984) Anatomy and physiology of a color system in the primate visual cortex. *Journal of Neuroscience* **4**:309-356.

McGuinness, E., C.T. McDonald, M.I. Sereno, and J.M. Allman (1986) Primates without blobs: The distribution of cytochrome oxidase activity in striate cortex in *Tarsius*, *Hapalemur*, and *Cheirogaleus*. *Society for Neuroscience, Abstracts* **12**:130.

Martin, R.D. (1990) *Primate origins and evolution*. Chapman & Hall.

Martin, R.D. (1993) Primate origins: plugging the gaps. *Science* **363**:223-234.

Murphy, K.M., R.C. Van Sluyters, and D.G. Jones (1990) Cytochrome-oxidase activity in cat visual cortex: is it periodic? *Society for Neuroscience, Abstracts* **16**:292.

Nadkarni, N.A., S. Bougacha, C. Garin, M Dhenain, and J.-L Picq (2019) A 3D population-based brain atlas of the mouse lemur primate with examples of applications in aging studies and comparative anatomy. *Neuroimage* **185**:85-95.

Neuenschwander, S., R. Gattass, A.P.B. Sousa, and M. C. G.P. Piñon (1994) Identification and visuotopic organization of areas PO and POd in *Cebus* monkey. *Journal of Comparative Neurology* **340**:65-86.

Olavarria, J. and R.C. Van Sluyters (1985) Unfolding and flattening the cortex of gyrencephalic brains. *Journal of Neuroscience Methods* **15**:191-202.

Palmer, L.A., A.C. Rosenquist, and R.J. Tusa (1978) The retinotopic organization of lateral suprasylvian visual areas in the cat. *Journal of Comparative Neurology* **177**:237-256.

Paolini, M., and M.I. Sereno (1998) Direction selectivity in the middle lateral and lateral (ML and L) visual areas in the California ground squirrel. *Cerebral Cortex* **8**:362-371.

Pettigrew, J.D. (1999) Electroreception in monotremes. *Journal of Experimental Biology* **202**:1447-1454.

Preuss, T.M. and J.H. Kaas (1996) Cytochrome oxidase 'blobs' and other characteristics of primary visual cortex in a lemuroid primate, *Cheirogaleus medius*. *Brain Behavior and Evolution* **47**:103-112.

Radinsky, L. (1967) The oldest primate endocast. *American Journal of Physical Anthropology* **27**:385-388.

Rosa, M.G.P., A.P.B. Sousa, and R. Gattass (1988) Representation of the visual field in the second visual area in the *Cebus* monkey. *Journal of Comparative Neurology* **275**:326-345.

Rosa, M.G.P., L.M. Schmid, L.A. Krubitzer, and J.D. Pettigrew (1993) Retinotopic organization of the primary visual cortex of flying foxes (*Pteropus poliocephalus* and *Peteropus scapulatus*). *Journal of Comparative Neurology* **335**:55-72.

Rosa M.G.P. and L.M. Schmid (1995) Visual areas in the dorsal and medial extrastriate cortices of the marmoset. *Journal of Comparative Neurology* **359**:272-299.

Rosenquist, A.C. (1985) Connections of visual areas in the cat. In E.G. Jones and A. Peters (eds.), *Cerebral Cortex,* Volume 3. Plenum Press, pp. 81-117.

Schwartz, J.H. (1986) Primate systematics and a classification of the order. In *Comparative Primate Biology, Volume 1: Systematics, Evolution, and Anatomy*, pp. 1-41.

Saraf, M.P., P. Balaram, F. Pifferi, R. Gamanut, H. Kennedy, and J.H. Kaas (2017) Architectonic features and relative locations of primary sensory and related areas of neocortex in mouse lemurs. *Journal of Comparative Neurology* **527**:625-639.

Scheich, H. G. Langner, C. Tidemann, R.B. Coles, and A. Guppy (1986) Electroreception and electrolocation in platypus. *Nature* **319**:401-402.

Sereno, M.I. and J.M. Allman (1991) Cortical visual areas in mammals. In A. Leventhal (ed.), *The Neural Basis of Visual Function, Vol 4, Vision and Visual Dysfunction*. J. Cronly-Dillon (gen. ed.). London: Macmillan, pp. 160-172.

Sereno, M.I., H.R. Rodman, and H.J. Karten (1991) Organization of visual cortex in the California ground squirrel. *Society for Neuroscience, Abstracts* **17**:844.

Sereno, M.I., C.T. MacDonald, J.M. Allman (1994) Analysis of retinotopic maps in extrastriate cortex. *Cerebral Cortex* 4:601-620.

Sereno, M.l., A.M. Dale, J.B. Reppas, K.K. Kwong, J.W. Belliveau, T.J. Brady, B.R. Rosen and R.B.H. Tootell (1995) Borders of multiple visual areas in human revealed by functional magnetic resonance imaging. *Science* **268**:889-893.

Sereno, M.I. and R.B.H. Tootell (2005) From monkeys to humans: what do we now know about brain homologies? *Current Opinion in Neurobiology* **15**:135-144.

Sereno, M.I., C.T. McDonald, and J.M. Allman (2015) Retinotopic organization of extrastriate cortex in the owl monkey -- dorsal and lateral areas. *Visual Neuroscience* **32**:e021, 39 pages.

Sur, M., R.J. Nelson, and J.H. Kaas (1978) The representation of the body surface in somatosensory area I of the grey squirrel. *Journal of Comparative Neurology* **179**:425-450.

Szalay, F. and E. Delson (1979) *Evolutionary History of the Primates*. Academic Press.

Tootell, R.B.H., S.L. Hamilton, and M.S. Silverman (1985) Topography of cytochrome oxidase activity in owl monkey cortex. *Journal of Neuroscience* **5**:2786-2800.

Tootell, R.B.H., K.K. Kwong, J.W. Belliveau, J.R. Baker, C.E. Stern, S.J. Hockfield, H. Breiter, R. Born, T.J. Brady, and B.R. Rosen (1993) Mapping human visual cortex: evidence from functional MRI and histology. *Investigative Ophthalmology and Visual Science* **34**:813 (Abstract).

Tusa, R.J. and L.A. Palmer (1980) Retinotopic organization of areas 20 and 21 in the cat. *Journal of Comparative Neurology* **193**:147-164.

Updyke, B.V. (1986) Retinotopic organization within cat's posterior suprasylvian sulcus and gyrus. *Journal of Comparative Neurology* **246**:265-280.

Van Essen, D.C., W.T. Newsome, J.H.R. Maunsell, and J.L. Bixby (1986) The projections from striate cortex (V1) to visual areas V2 and V3 in the macaque monkey: asymmetries, areal boundaries, and patchy connections. *Journal of Comparative Neurology* **244**:451-480.

Wessel, P. and W.H.F. Smith (1991) Free software helps map and display data. *EOS Transactions, American Geophysical Union* **72**:441-446.

Wong, P. and J.H. Kaas (2010) Architectonic Subdivisions of Neocortex in the Galago (*Otolemur garnetti*). *The Anatomical Record* **293**:1033–1069.

Yoder, A.D. (1992) The applications and limitations of ontogenetic comparisons for phylogeny reconstruction: the case of the strepsirhine internal carotid artery. *Journal of Human Evolution* **23**:183-195.

Yu H.-H., D.P. Rowley, N.S.C. Price, M.G.P. Rosa (2020) A twisted visual field map in the primate dorsomedial cortex predicted by topographic continuity. *Science Advances* **6**:eaaz8673